

Lawrence Berkeley National Laboratory

Recent Work

Title

Carbon Dioxide Plume Evolution Following Injection into a Depleted Natural Gas Reservoir:
Modeling of Conformance Uncertainty Reduction Over Time

Permalink

<https://escholarship.org/uc/item/1wv2g0ng>

Authors

Doughty, Christine
Oldenburg, Curtis

Publication Date

2019

Peer reviewed

2
3 Carbon Dioxide Plume Evolution Following Injection into a Depleted Natural Gas Reservoir:

4 Modeling of Conformance Uncertainty Reduction Over Time

5
6 Christine Doughty and Curtis M. Oldenburg

7 Earth and Environmental Sciences, Lawrence Berkeley National Laboratory

8 Berkeley, CA 94720 USA

9
10
11
12 August 15, 2019

13
14
15 Keywords: Geologic carbon sequestration; post-injection site care, uncertainty, conformance,
16 Class VI; depleted gas reservoir
17

Abstract

The uncertainty in the long-term fate of CO₂ injected for geologic carbon sequestration (GCS) is a significant barrier to the adoption of GCS as a greenhouse gas emission mitigation approach for industry and regulatory agencies alike. Here we present a modeling study that demonstrates that the uncertainty in forecasts of GCS site performance decreases over time as monitoring data are used to inform and update operational models. The approach we take is to consider a case study consisting of a depleted natural gas reservoir that is used for GCS with CO₂ injection occurring over 20 years, with a 50-year post-injection site care (PISC) period. We constructed a detailed model of the system and ran this model out to 200 years to generate the *actual* site data. A series of simpler *operational* models based on limited data and assumptions about how an actual operator would model such a site are then run and compared against the actual model output at various specific monitoring points after one year, two years, etc. The operational model is then updated and improved using the observations (synthetic data from the actual model) at the same time intervals. We found that both model parameter values and model features needed to be added over time to improve matches to the actual system. These kinds of model adjustments are expected to be a normal part of reservoir engineering and site management at GCS sites. We found that the uncertainty in two key measures related to site performance at various locations decreases with time. This overall conclusion should help allay the concerns of industry and regulators about the uncertainty in GCS operations.

1. Introduction

In order to make a substantial impact in reducing greenhouse gas emissions, geologic carbon sequestration (GCS) will need to involve injection of millions of tonnes of CO₂ at many sites worldwide over several decades. Following injection there will be a post-injection site care

(PISC) period during which monitoring will be carried out so that the operator can ensure that CO₂ storage is permanent and that the project is not impacting underground sources of drinking water (USDW). The U.S. EPA in its Class VI CO₂ injection well permitting regulation specifies 50 years as a period over which monitoring should be carried out during PISC (EPA, 2008), while the California Air Resources Board (2017) is currently suggesting a period of 100 years is needed for monitoring to ensure permanence. Given the lack of experience with industrial-scale CO₂ injection for GCS, the costs of multi-decadal monitoring operations during PISC are difficult to forecast, and this uncertainty is increasing the estimated lifecycle cost of GCS. Given the widespread agreement that GCS must be part of the solution for reducing effective greenhouse gas emissions (IPCC, 2018), there is strong motivation to understand more about the long-term evolution of injected CO₂ in the subsurface and the evolution of uncertainty in CO₂ storage as large-scale projects mature over time.

To address the above lack of knowledge, we have undertaken a modeling and simulation study that makes use of a synthetic GCS project about which everything is known by virtue of detailed numerical simulations. However, in this approach we assume that our knowledge of the GCS project is limited to model results that represent observations made at a limited number of monitoring wells, for a limited period of time. This limited information is used to develop a series of operational model of the GCS project, whose long-term predictions for CO₂ plume evolution are then compared with those of the detailed model representing the actual system. In this study, this procedure is repeated periodically, with more synthetic data becoming available as time progresses. The idea is that by examining synthetic monitoring data from the virtual GCS project at a series of times, we can determine how operational models improve over time as more data become available, and thereby reduce forecast uncertainty over time. With this

understanding of uncertainty evolution in hand, we can make recommendations about how much uncertainty there is in typical model-based forecasts of CO₂ plume and pressure evolution and how uncertainty evolves over time for the given injection scenario.

The example studied here considers a depleted natural gas reservoir system typical of large GCS opportunities in the Sacramento River Delta region of California. It was previously suggested that depleted gas reservoirs are, by virtue of their proven capacity to store a buoyant gas (i.e., methane), low-hanging fruit for large-scale GCS (Oldenburg et al., 2001). The objective of this study is to demonstrate the reduction in uncertainty over time of forecasts of plume properties as the updated operational models incorporate more field observational data and become more detailed and skilled at forecasting over time. We will show that not only does the uncertainty in forecasts of plume extent and pressure rise decrease, but so too will associated estimates of risk. The overall impact of these findings may have bearing on the time periods required for PISC. In addition, our study informs the needed monitoring intensity and related costs which also may be confidently estimated to decline with time based on our study. Finally, results of the study may cause risk-averse stakeholders to gain tolerance for uncertainty in early forecasts of a GCS project, knowing uncertainty will diminish over time.

2. Background

A survey of the literature on uncertainty reduction in GCS and other hydrologic systems uncovers a large body of research based on sophisticated approaches such as modified Kalman filters (Chen and Zhang, 2006; Sun et al., 2009), enhanced Monte Carlo methods (Keating et al., 2010), and polynomial chaos expansion (Oladyshkin et al., 2011; Walter et al., 2012). Our study does not utilize any sophisticated, elegant, or new techniques. The novelty is instead in the use of

a large synthetic system as a proxy for a real system, and the application to GCS where there is an urgent need for understanding of long-term evolution of model forecast uncertainty. Our study is also novel in that we couch uncertainty reduction in forecasts of CO₂ storage risk in terms of reduction in uncertainty of conformance.

In order to make the approach and findings of this study concise, it is useful to introduce the concept of conformance, which combines concordance and performance (e.g., Chadwick and Noy, 2015; Oldenburg, 2018). In the GCS context, concordance is the degree to which model forecasts of plume extent, pressure rise, etc. match observations, and performance is the degree to which the storage system is performing as designed. For example, models should be able to history-match observations (known in some fields as hindcasting), and the monitoring system should be indicating that CO₂ is filling the intended storage reservoir, not leaking, not impacting underground sources of drinking water (USDW), and not causing pressure rise above tolerable ranges. If all of these conditions are met, we can say the system is conforming. In terms of regulators and stakeholders, a conforming GCS project is a successful GCS project.

Nevertheless, as with all subsurface technologies, there is uncertainty involved in the assessment of conformance, and this uncertainty must be understood in order to understand the robustness of conformance assessment (e.g., Harp et al., 2019).

Further to the above, we address in this study the reduction in uncertainty in forecasts of conformance. Conformance forecasts are uncertain because the underlying model predictions are uncertain. In the present study, we use synthetic system performance data to quantify the uncertainty in operational model forecasts and make conclusions about how that uncertainty diminishes over time in a project as the operational model improves as experience with the system is accumulated. Therefore, this study addresses the question of the reduction in

uncertainty (during GCS operations as models are improved) of forecasts of conformance. Additional uncertainty enters into conformance assessments from the incomplete knowledge arising from imprecise monitoring observations. We have not included this aspect into the study in order to focus attention on the uncertainty that diminishes as experience with a system is gained over time and as that experience is incorporated into operational models.

3. Approach

The approach we take involves use of a detailed model of a GCS scenario at a site to generate a set of synthetic data that constitute the *actual* system. This actual system includes several monitoring wells from which discrete observational data are assumed to be known from monitoring. We assume that the operators of the project would have an *operational* model of the CO₂ injection and storage system that they use for injection design, risk assessment, monitoring design, and permitting. Assuming the project is permitted and injection begins, observations and performance data would be used to update the operational model. This study carries out this observation-model update loop to demonstrate the reduction in uncertainty of model forecasts over time. The procedure is outlined in flow chart form in Figure 1 where the CO₂ injection period is 20 years and the PISC period is assumed to be 50 years following the U.S. EPA Class VI regulation (U.S. EPA, 2008).

We first define an injection scenario and design a logical and practical monitoring program. We then create a detailed numerical model and simulate 20 years of large-scale CO₂ injection and 180 years of shut-in to create a synthetic “actual” case of performance and monitoring data. This synthetic data set is then set aside. Using a subset of characterization data, we then create a simplified operational model conceived as being similar to one that an actual operator would

develop based on available data, which are assumed to be much more limited than the data that went into defining the actual model. As shown in the flowchart of Figure 1, we use the operational model to simulate injection and monitoring for the first year. Based on a comparison of operational model monitoring observations to actual model monitoring observations (assumed to be 100% correct, i.e., no measurement uncertainty) at discrete monitoring well locations at the end of Year 1, we then adjust the simplified operational model (history match) and make a forecast for Year 2. We then repeat this process over the years of injection (see Figure 1). We demonstrate by this approach that the simplified operational model becomes better and better over time (uncertainty decreases) in making long-term forecasts, as observations are incorporated into the model to improve its annual forecasting skill.

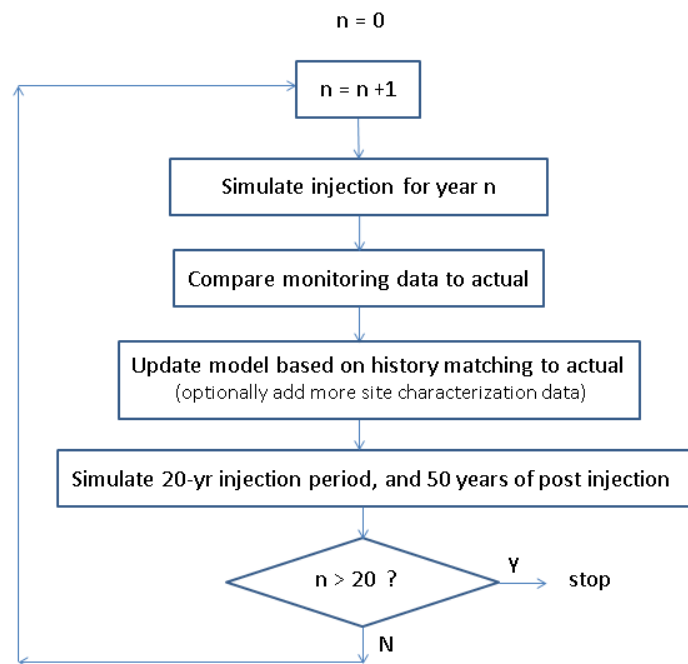


Figure 1. Flow chart showing the updating and forward simulation steps for the operational model used in the study.

Actual Depleted Gas Reservoir System

California Delta Geologic Setting

The simulated system we use as the actual model has properties based on a site that is representative of typical large-scale depleted natural gas (CH_4) reservoirs in the Sacramento River Delta area of California. This region in the southwestern Sacramento Valley is within 50 miles (80 km) of several San Francisco Bay Area refineries that may someday capture CO_2 for GCS. An unpublished regional-scale geologic model (see Burton et al., 2016) provides the overall geologic structure. The sandstone storage reservoir we consider has variable thickness averaging approximately 500 m at depths of 1000-2000 m. The storage reservoir is composed of high-permeability sandstone with local low-permeability zones; it is generally dipping at 1.6° to the SW, and is capped by an impermeable shale over an undulating reservoir top surface. Layering within the sandstone storage reservoir is based on a well log (Figure 2) from a Sacramento River Delta well (Burton et al., 2016), and we add stochastic heterogeneity to each model layer using GSLIB (Deutsch and Journel, 1992) (Figure 3). Two sub-vertical faults are included that inhibit cross-flow, but enhance flow parallel to the faults. The depth of the top of the storage formation is shown in Figure 4, revealing the dip and attic regions in the storage reservoir. The brine in the system initially is assumed to contain dissolved CH_4 , consistent with it being a depleted gas reservoir. While many of the larger natural gas reservoirs in the Sacramento River Delta area are depleted, free-phase CH_4 is often still present in localized attic regions trapped up against the caprock (Figure 5) and we assume that is the case here. As shown below, injected CO_2 buoyantly pinned in the upper-most regions of the storage reservoir will tend to migrate NE toward the shallowest regions and into attics in the reservoir that contain residual free-phase CH_4 .

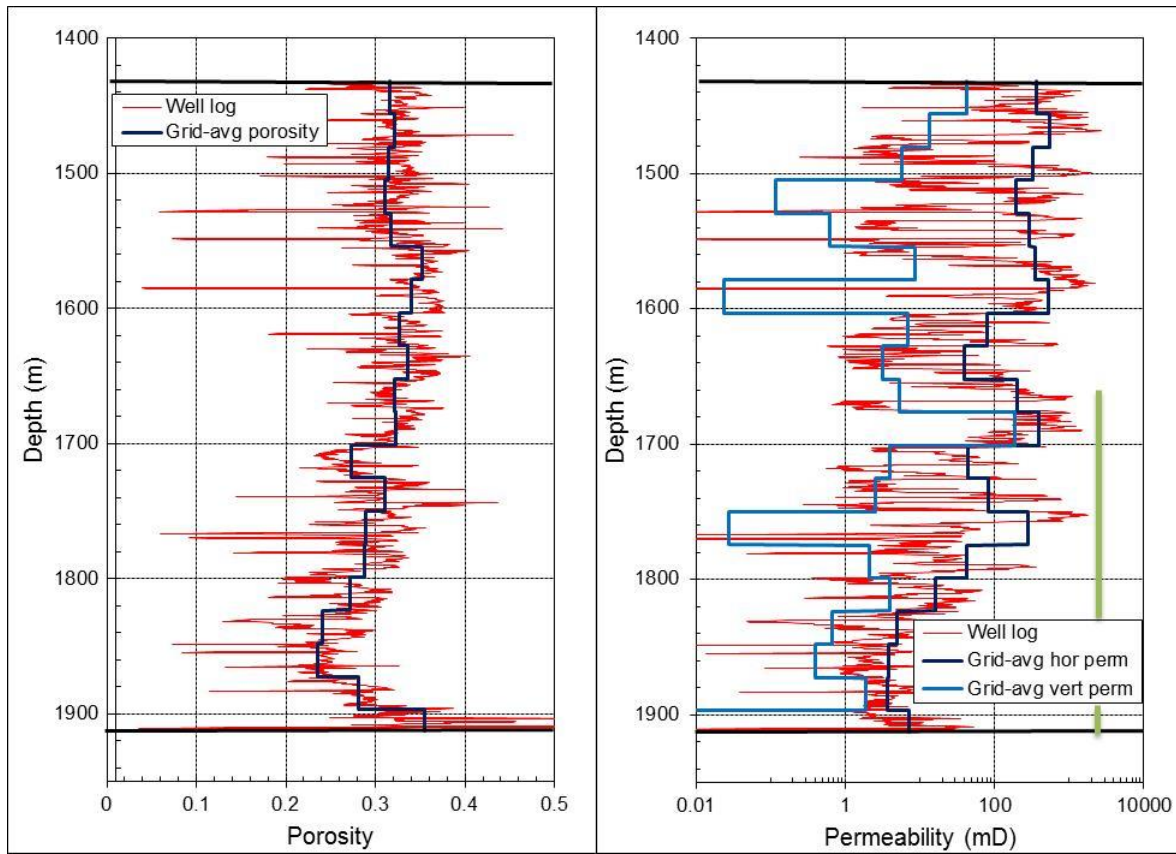


Figure 2. Well-log data used to determine layer porosities and permeabilities at the injection well in the actual model. The perforated interval is shown as a green bar.

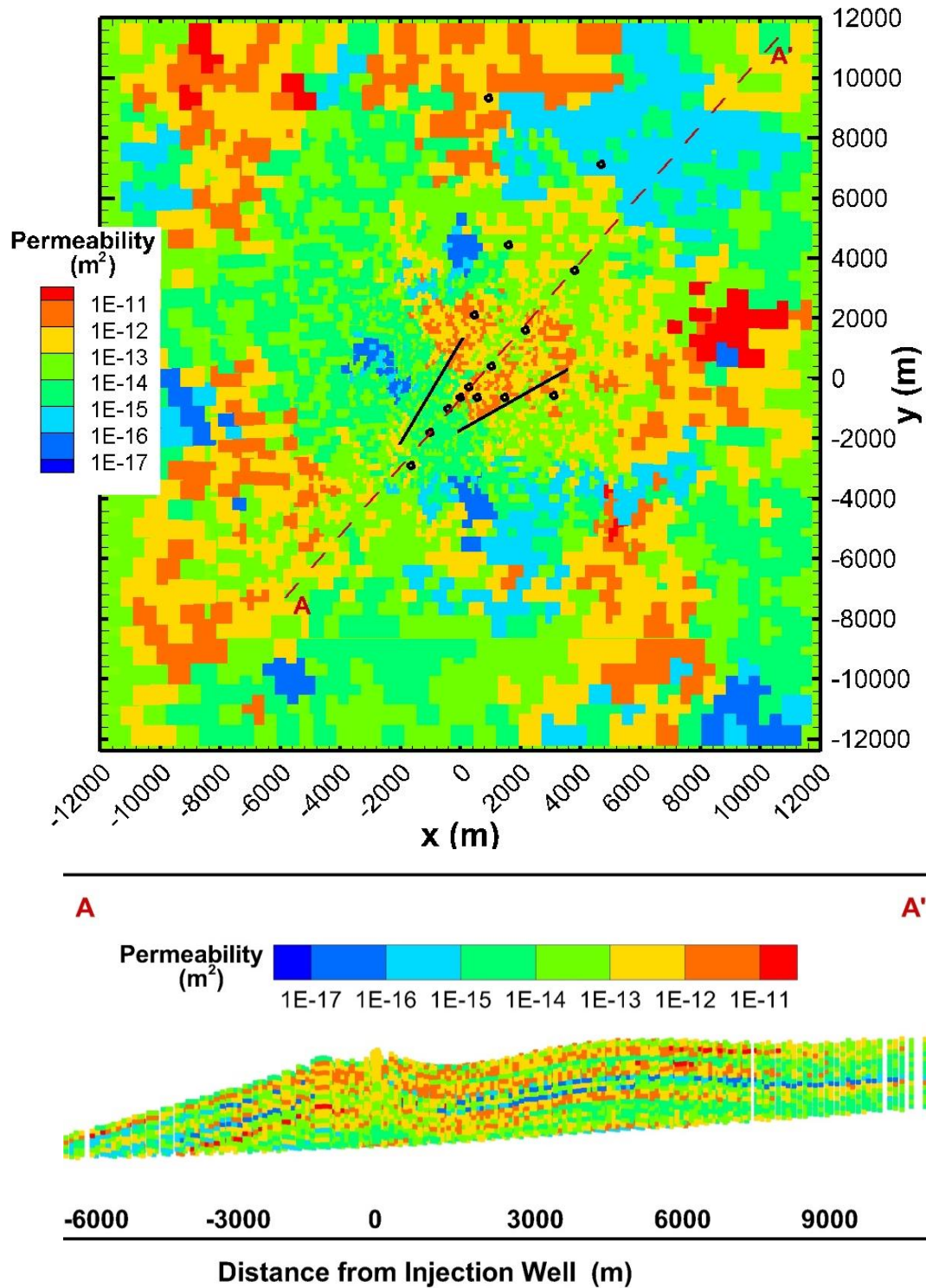
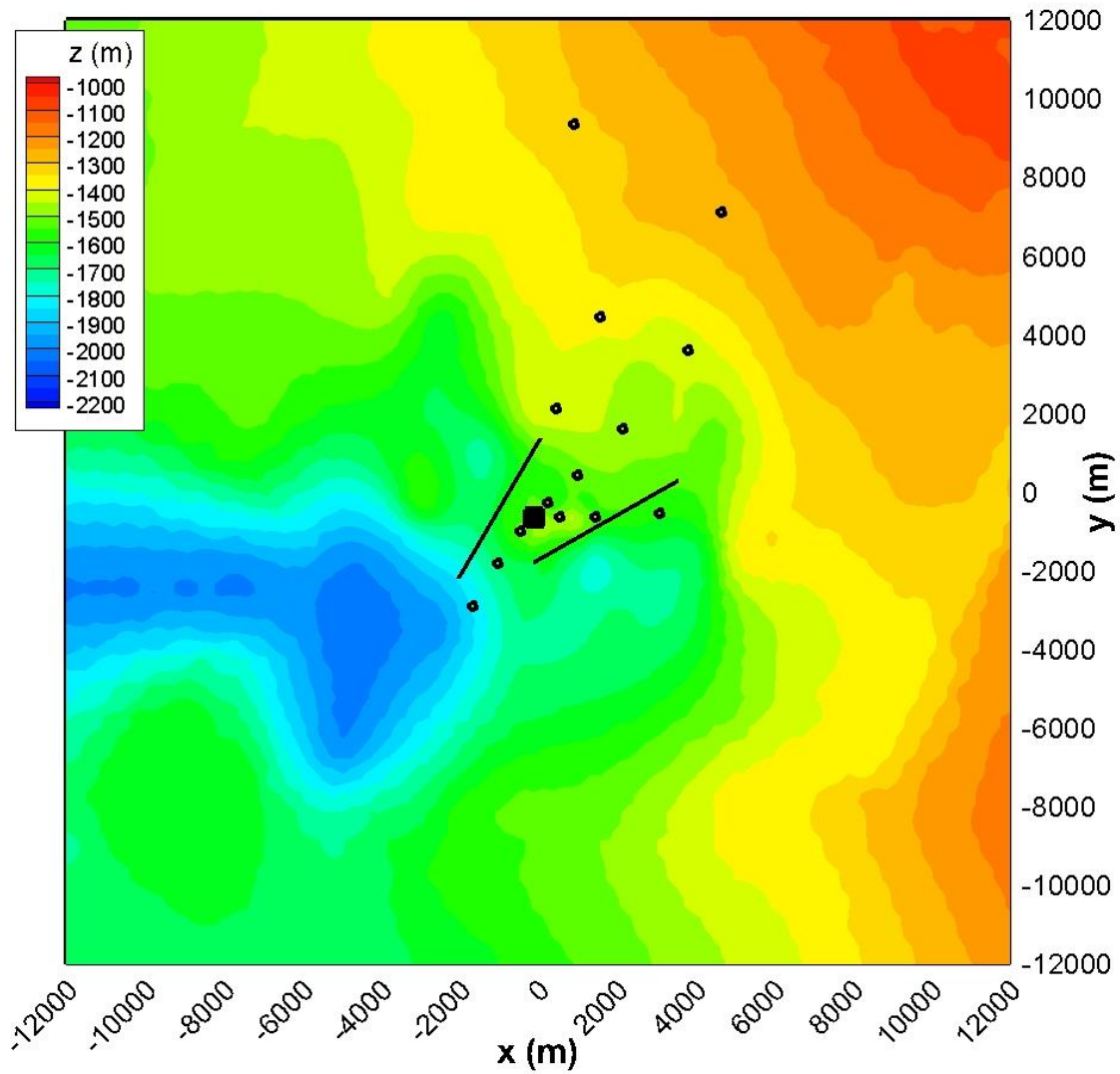


Figure 3. (top) The center region of the top layer of the storage reservoir in the actual model, illustrating the heterogeneous permeability distribution along with monitoring wells (black circles). Two vertical faults are shown as black line segments. (bottom) Vertical cross-section at the location of the dashed line shown in the top frame showing the reservoir heterogeneity and locally closed structures (attics). Vertical exaggeration is two times.



179
180

181 *Figure 4. Elevation of the top of the storage formation assuming ground surface is at $z = 0$ m.*
 182 *The injection well (black square) is NE of a deep pendant of the caprock (blue region). Buoyancy*
 183 *is expected to carry CO_2 to the NE toward the yellow and reddish colored attics of the reservoir.*

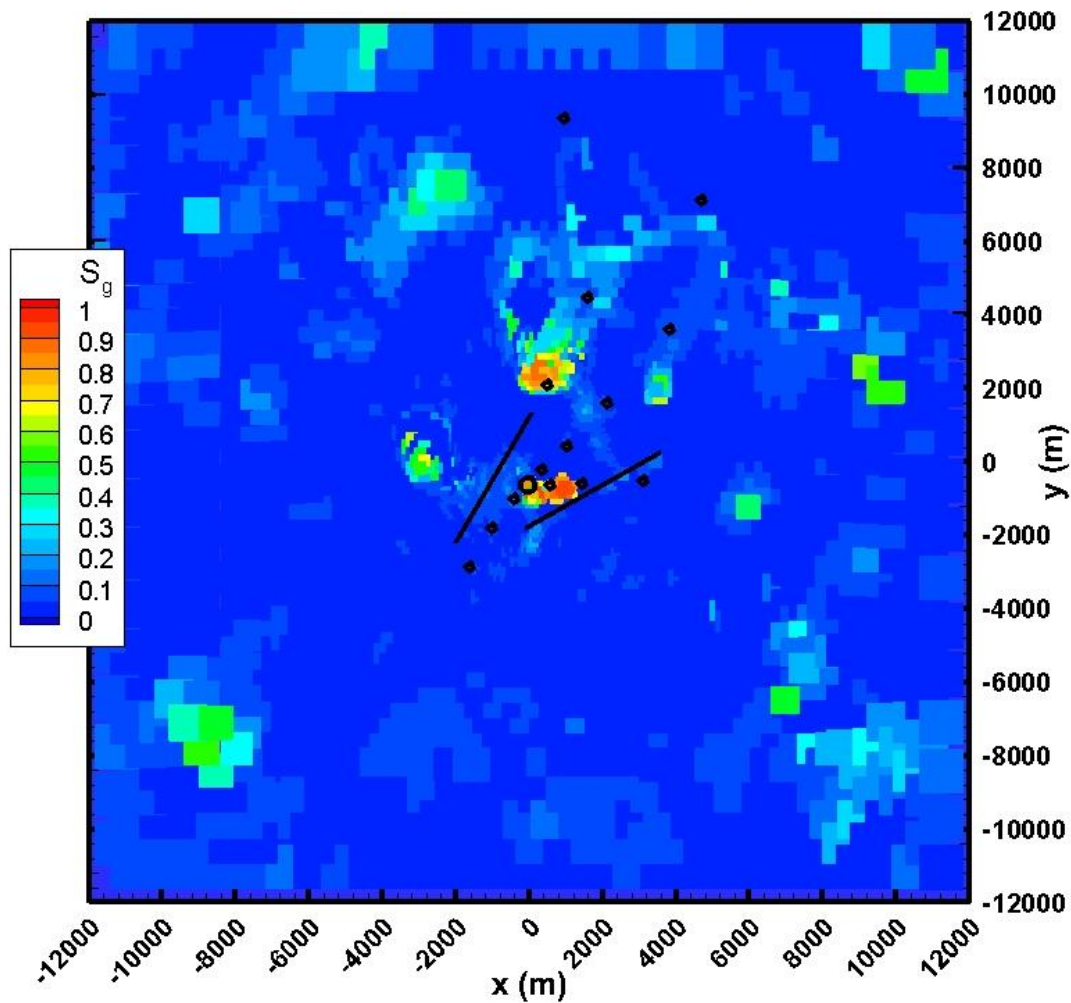


Figure 5. Initial saturation conditions in the actual model showing free-phase CH_4 localized in attic regions by buoyancy forces.

Injection and Monitoring Scenario

The scenario simulated specifies 8 Mt/yr of CO_2 injection for 20 years, and we run the simulation out another 180 years to observe very long-term evolution. Injection is into the lower half of the storage reservoir allowing for buoyant rise of injected CO_2 up into the attic regions of the reservoir. Studies such as Foxall et al. (2017) found that in highly permeable California Delta

sandstones, one well was sufficient to inject at this rate (i.e., near-well pressure remains below frac pressure). The injection well and 14 monitoring wells are included in the model to serve as points in the system where measurements of pressure, saturation, and gas composition are assumed to be made over time (Figure 6). At the injection well (I) and at nine nearby monitoring wells (D, L, U wells, named for their general locations downstream, lateral, and upstream relative to the injection well), we assume monitoring is done at two depths: (1) top of the perforated interval, and (2) top of the storage reservoir. At five more-distant wells (F wells, named for being far from the injection well), we assume monitoring is done only at the top of the storage reservoir. The total number of monitoring wells assumed here is probably unrealistically large (i.e., more than would be installed in any actual project, especially in the early stages of injection), but for this simulation study we need good spatial coverage to demonstrate how pressure and saturation change in the system for the entire project period. While pressure is assumed to be available continuously, saturation measurements (e.g., obtained using a pulsed neutron logging technique such as Schlumberger's time-lapse Reservoir Saturation Tool (RST)) and fluid sampling to measure gas- and liquid-phase composition, e.g., by U-Tube sampling (Freifeld et al., 2005), could be carried out at discrete times. Although not used for the present study, continuous temperature measurements are straightforward to make, and would likely be part of any monitoring dataset at GCS sites.

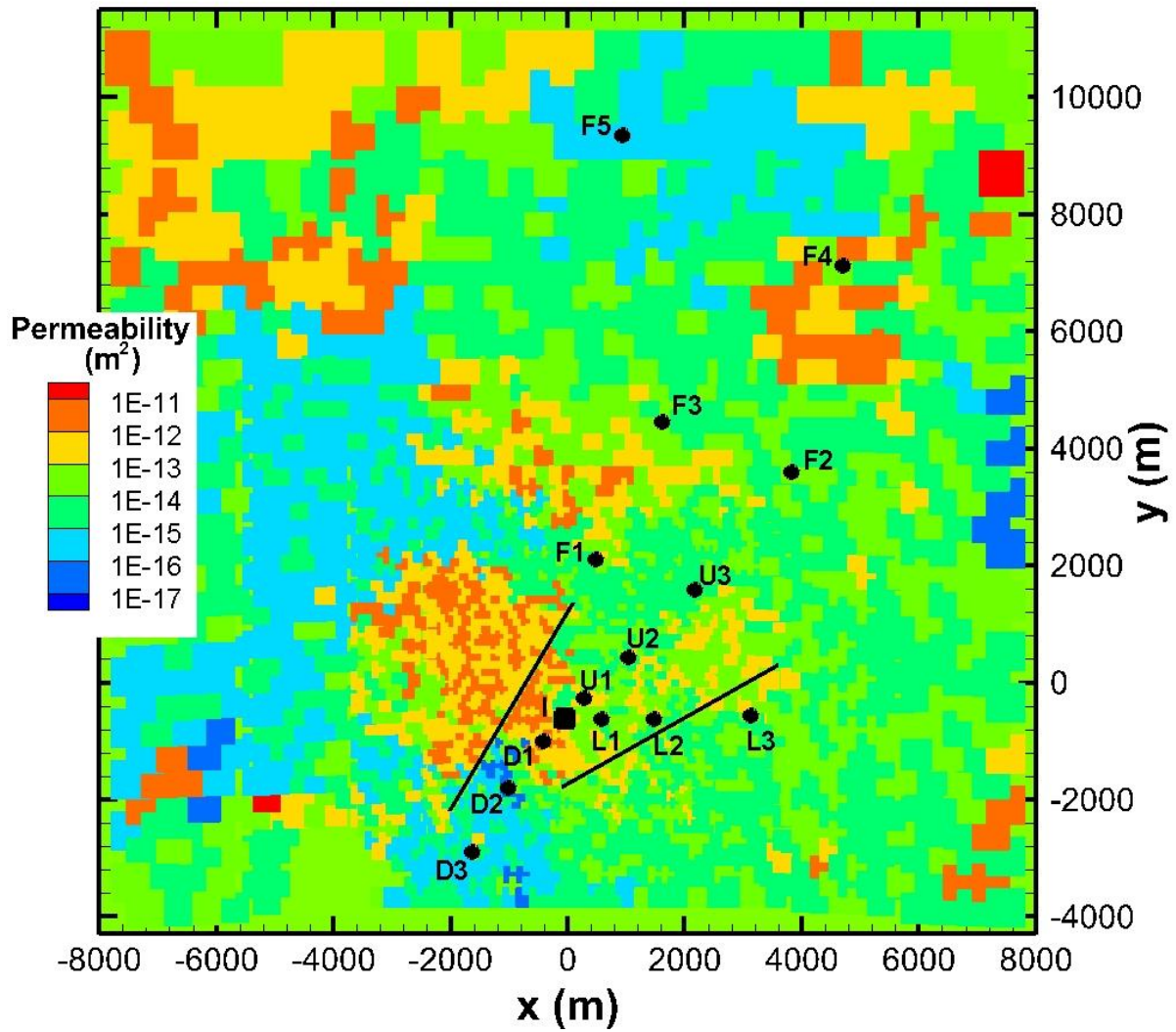


Figure 6. The injection well (square) and monitoring well layout. The background shows the permeability distribution in the fourth layer of the reservoir in the actual model to illustrate the vertical variation compared to the top layer shown in Figure 3.

Domain Discretization

In plan view, the model domain is 47 km by 60 km as shown in Figure 7. We discretized the domain finely around the injection and monitoring wells, and gradually coarsened the grid toward the boundaries. Hexagonal grid blocks are used to reduce grid-orientation effects. The

220 west and south boundaries are approximately aligned with regional faults that are assumed to be
221 impermeable to trans-fault flow. The east (right-hand side) boundary is up-dip and open to flow,
222 while the north boundary is closed. Vertical discretization (Figure 7) follows layers from the
223 geologic model (see Burton et al., 2016) with variable thickness layers that can pinch out. The
224 grid for the storage formation has 20 layers at the injection well, and 30 layers at its thickest
225 point.

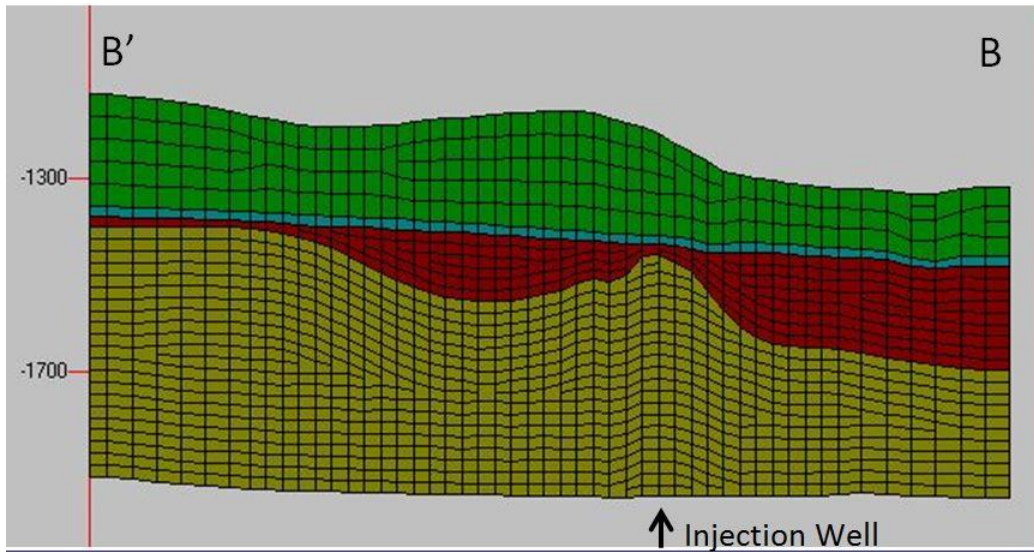
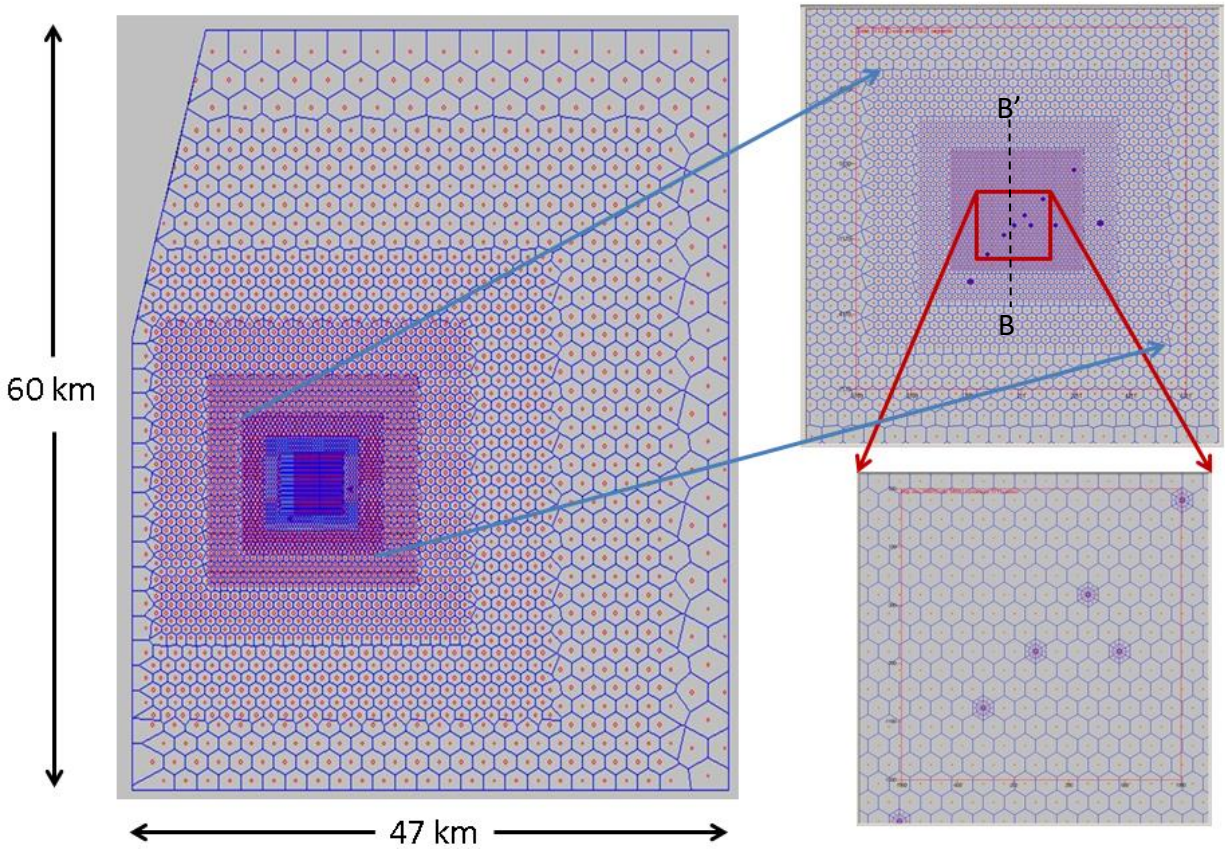


Figure 7. (top) Map view of 3D grid showing grid refinement around injection and monitoring wells that are roughly aligned with the expected plume migration path updip (see Figure 4); (bottom) N-S cross-section passing close to the injection well. Vertical exaggeration is five times. Yellow color shows the storage formation, red and blue are low-permeability seals, and green is an overlying aquifer.

Operational Model System

It is important to remember that the model described above was created to generate the synthetic data (i.e., describing the actual system) that will be compared to a series of subsequent models.

We will refer to the two classes of models as the actual model and the operational model, respectively. The operational model is developed to mimic the kind of model that operators of the site would use to design the injection scenario, design monitoring plans, estimate Area of Review (AoR), obtain their injection permit(s), and manage ongoing operations. The first operational model is based on data available prior to injection. Moreover, the first operational model and its early updates may be developed based on subsets of all of the monitoring wells that are ultimately installed (i.e., early operational models will be developed prior to all of the wells being installed), again resulting in reliance on a limited set of data. In general, the operational model will be simpler and more generalized early in a project and become more detailed and accurate later in the project. The present study is aimed at demonstrating such improvement and corresponding reduction in uncertainty of model results and forecasts.

The operational model utilizes the same grid and boundary conditions as the actual model. But we assume that early in the project the operators would simplify the reservoir system and assume it to be homogeneous. Furthermore, complexities like hysteresis in relative permeability and capillary pressure would likely be omitted due to lack of data. Similarly the inclusion of residual CH_4 in the system is a complication that would likely be left out for simplicity in early operational models. In Table 1, we summarize the properties of the actual and operational models. The years at which various features were added to the operational models are also shown; the rationales for these additions are described in the next section.

256 *Table 1. Properties of the actual model and the initial operational model.*

Model Feature	Actual Model	Initial Operational Model	When Features Added
Formation Geometry	From geologic model: dipping storage formation about 500 m thick; lateral extent: 47 km by 60 km; undulating caprock/formation interface	Same as Actual Model	Year 0 (initial)
Lateral Boundary Conditions	Three closed lateral boundaries represent sealing faults, open updip lateral boundary represents transition to a shallower aquifer system	Same as Actual Model	Year 0 (initial)
Layering	20 layers from well log, range of ϕ : 0.24 – 0.35, range of k_h : 3.7 – 551 mD, range of k_v : 0.008 – 188 mD	No layers: uniform $\phi = 0.3$, $k_h = 24$ mD, $k_v = 1.2$ mD	Year 1
Faults	Two vertical faults, $k_h = 5$ mD, $k_v = 200$ mD	No faults	1st fault -Year 2, 2nd fault -Year 10
Lateral Heterogeneity	Stochastic heterogeneity (GSLIB, Deutsch and Journel 1992); permeability roughly log-normal, conditioned to well log, range of ϕ : 0.025 – 0.56, range of k_h : 0.015 mD – 68 D, log-mean $k_h = 22$ mD; range of k_v : 0.014 nD – 63 mD	None	
Multi-phase flow properties	Hysteretic van Genuchten (Doughty, 2007); S_{lr} , m , S_{grmax} depend on permeability: range of $S_{lr} = 0.03 – 0.42$, range of m : 0.86 – 1.25, range of $S_{grmax} = 0.027 – 0.50$; Leverett scaling for P_{c0}	Non-hysteretic van Genuchten (1980): $S_{lr} = 0.116$, $m = 1.052$, $S_{gr} = 0$ during injection period; $S_{gr} = 0.2$ during post-injection period	Year 25, Year 50
Initial Conditions	Hydrostatic pressure distribution, geothermal temperature gradient, gas-phase CH ₄ in localized attics up against lower-most caprock	Same but no CH ₄	Year 5

4. Results

Actual Model

Complete information

Figure 8 shows layer and cross-section views of the CO₂ plume at the end of the injection period, 20 years, and at the end of the extended simulation at 200 years. Note that CO₂ moves readily upward in the formation from the perforated interval to the top of the formation. As the CO₂ plume develops, it is surrounded by a halo of free-phase CH₄, which forms when CH₄ dissolved in the brine exsolves into the gaseous phase provided by the injected CO₂ (e.g., Oldenburg et al., 2013).

Figure 9 shows the maximum pressure change in the uppermost layer of the storage formation which occurs at the end of the injection period. The black contour line indicates a pressure change of 0.1 MPa, which would be sufficient to lift fluid 10 m.

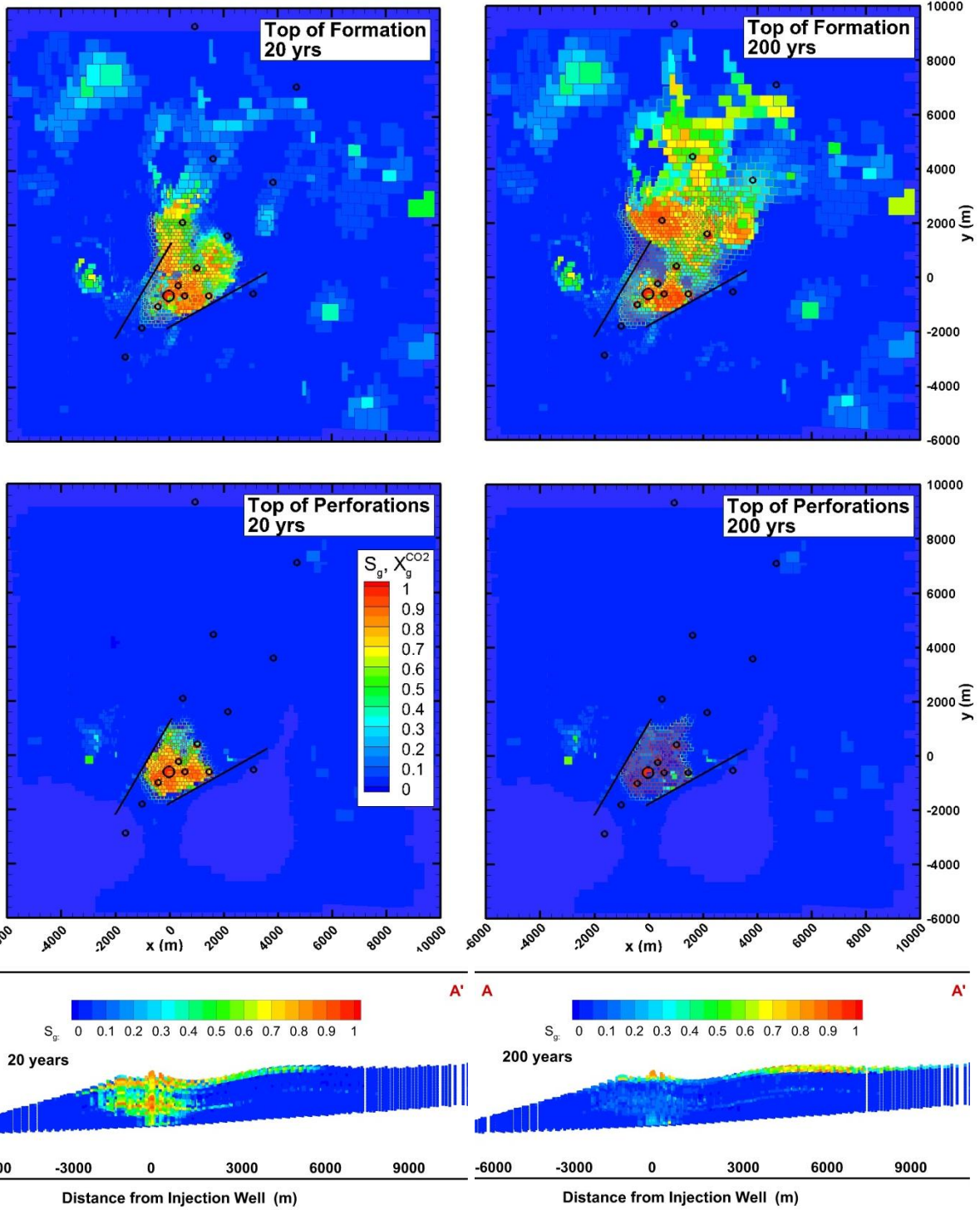
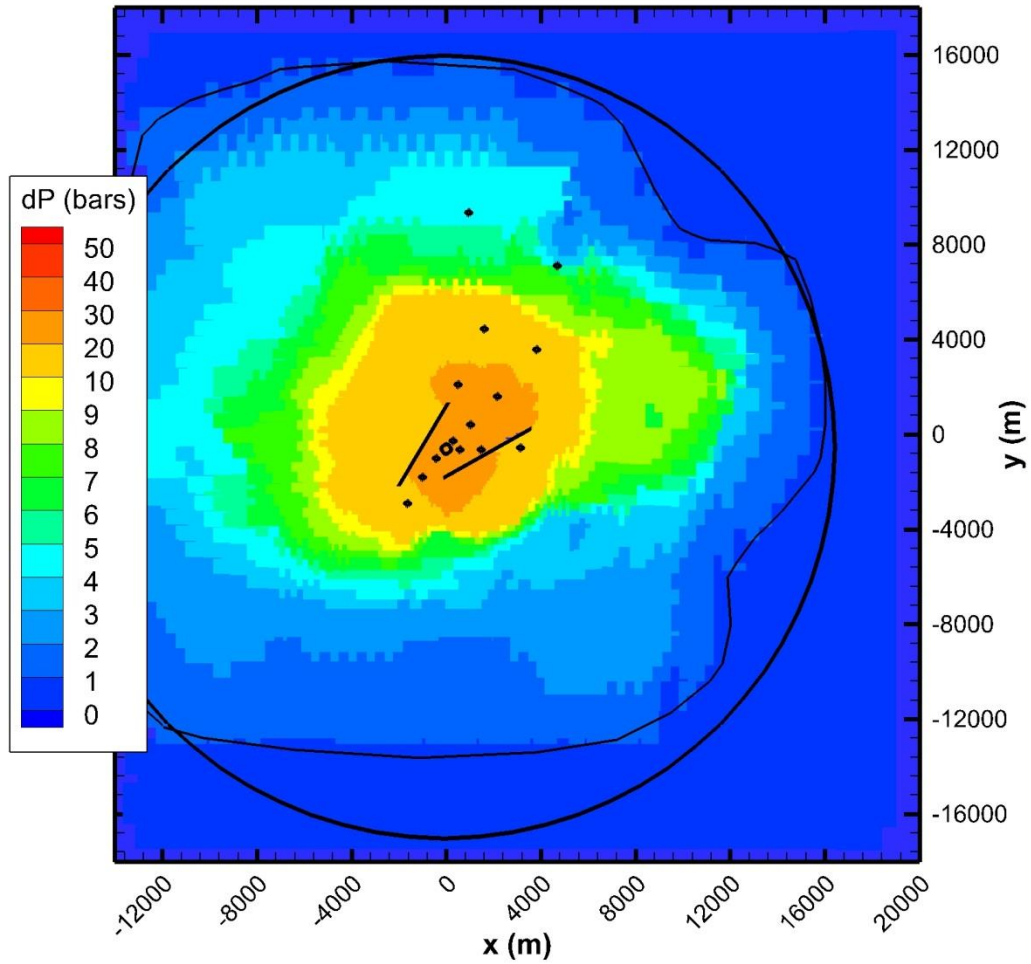


Figure 8. Distribution of CO_2 at the end of the injection period (eft column) and at the end of the simulation (right column). In the top four frames, the cell fill color indicates gas saturation and the cell outline color indicates CO_2 mass fraction. The location of the cross-sections is shown in Figure 3.



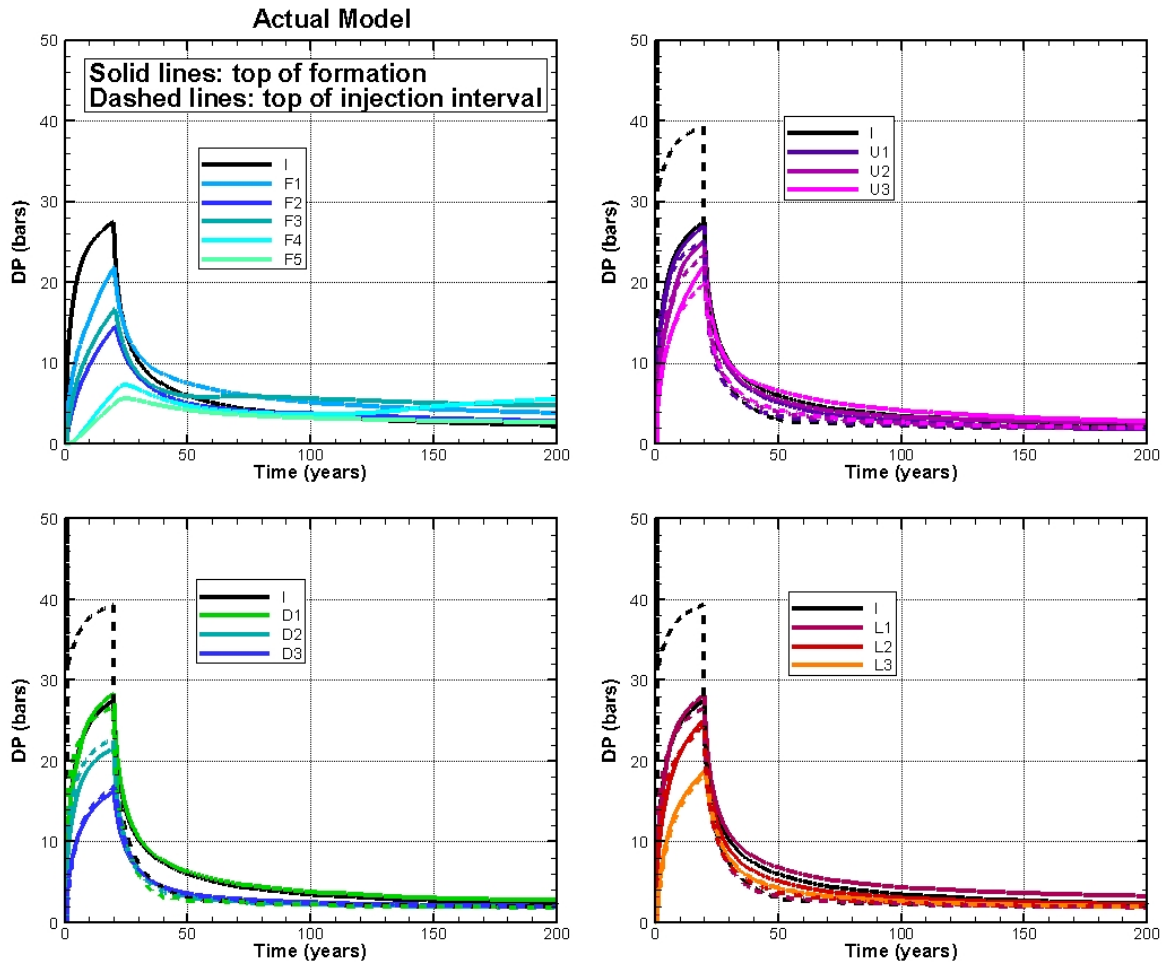
278

279 *Figure 9. The layer at the top of the storage formation, showing the pressure increase at the end*
 280 *of the injection period. The thin black line outlines the region with $dP > 1$ bar and the thick*
 281 *black line approximates this region with a circle of radius 16.5 km.*

282 **Monitoring Data**

283 Figures 8 and 9 provide a complete view of the evolution of the CO₂ plume and pressure pulse,
 284 but we will not use these data in operational model development. Rather, to demonstrate the
 285 evolution of conformance uncertainty over time, we limit ourselves to monitoring data that
 286 would be obtained from monitoring wells consisting of pressure transients (Figure 10) and
 287 saturation profiles (Figures 11 and 12). Moreover, we do not use the entire 200-year duration of

288 these data, but just the portion up to the year in which the model development is occurring. All
289 wells show pressure changes very soon after injection starts (Figure 10), but saturation changes
290 occur later at more distant monitoring wells (Figure 11). The sequence of saturation changes at
291 the injection well (Figure 12) is typical of the nearby monitoring wells, in that the first response
292 is at the depth of the perforated interval, with upward movement of the CO₂ plume occurring
293 later during the injection period and continuing through the full simulation period. In contrast, in
294 more distant monitoring wells, the CO₂ plume arrives in the uppermost portion of the storage
295 formation and stays there at all subsequent times.



296

297 *Figure 10. Actual model pressure transients. Legends show well names; see Figure 6 for*
 298 *locations. The upper left frame shows the far wells, and the other three frames show the U, D,*
 299 *and L wells. The injection-well response is shown in each frame for reference. Dashed and solid*
 300 *lines show the response at the top of the perforated interval and the top of the storage formation,*
 301 *respectively.*

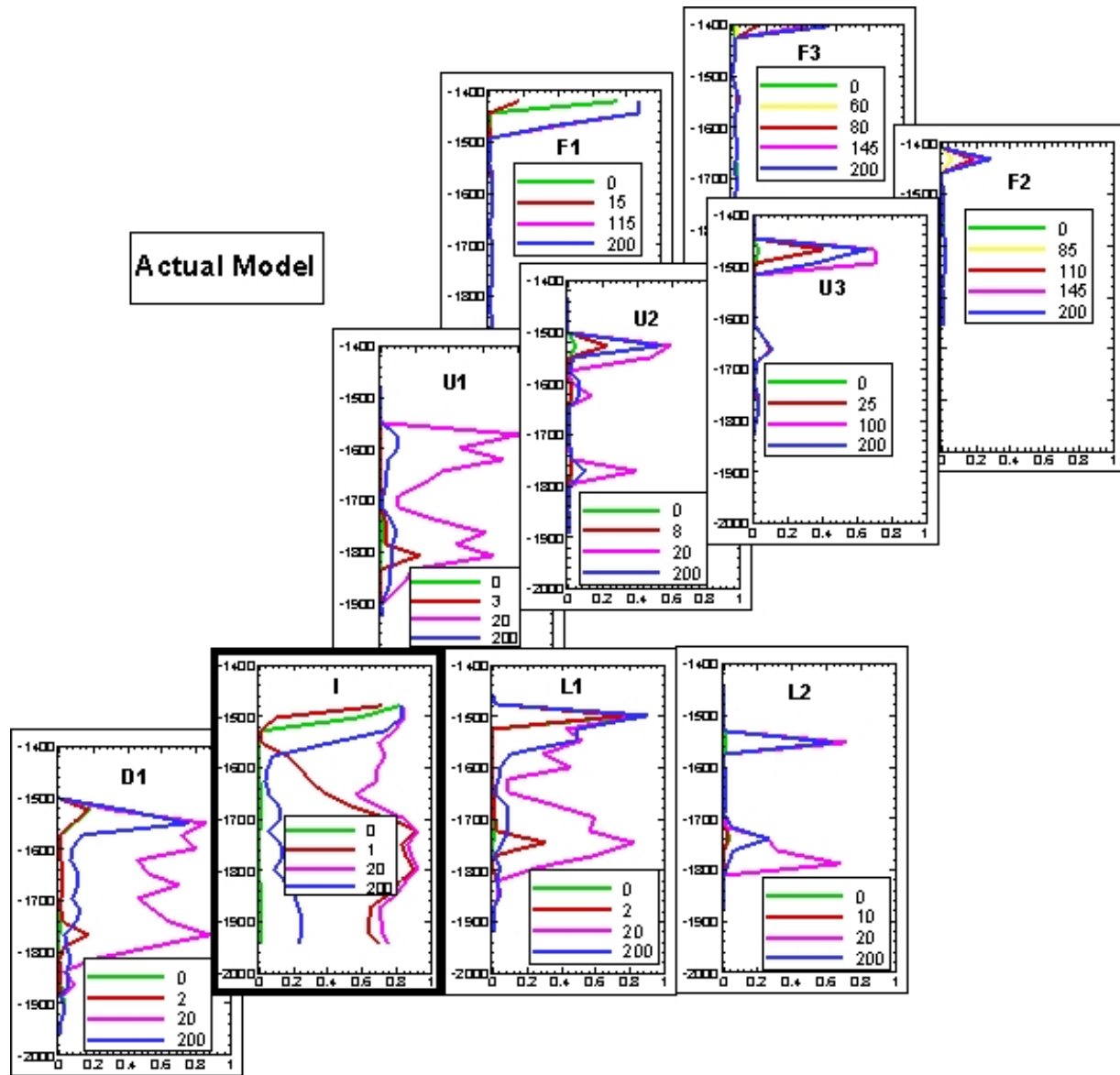


Figure 11. Selected saturation profiles in the monitoring wells for the actual model: green is the initial condition (gas is CH_4), yellow shows first increase in CH_4 , red shows first increase in CO_2 , pink is the maximum S_g , and blue is the final condition at 200 years. Of the 15 wells available for monitoring, saturation changes are only observed in these 10 wells. X axis is gas saturation S_g ; Y axis is depth in meters; legend is profile time in years. The layout of profile plots corresponds to well location (Figure 6).

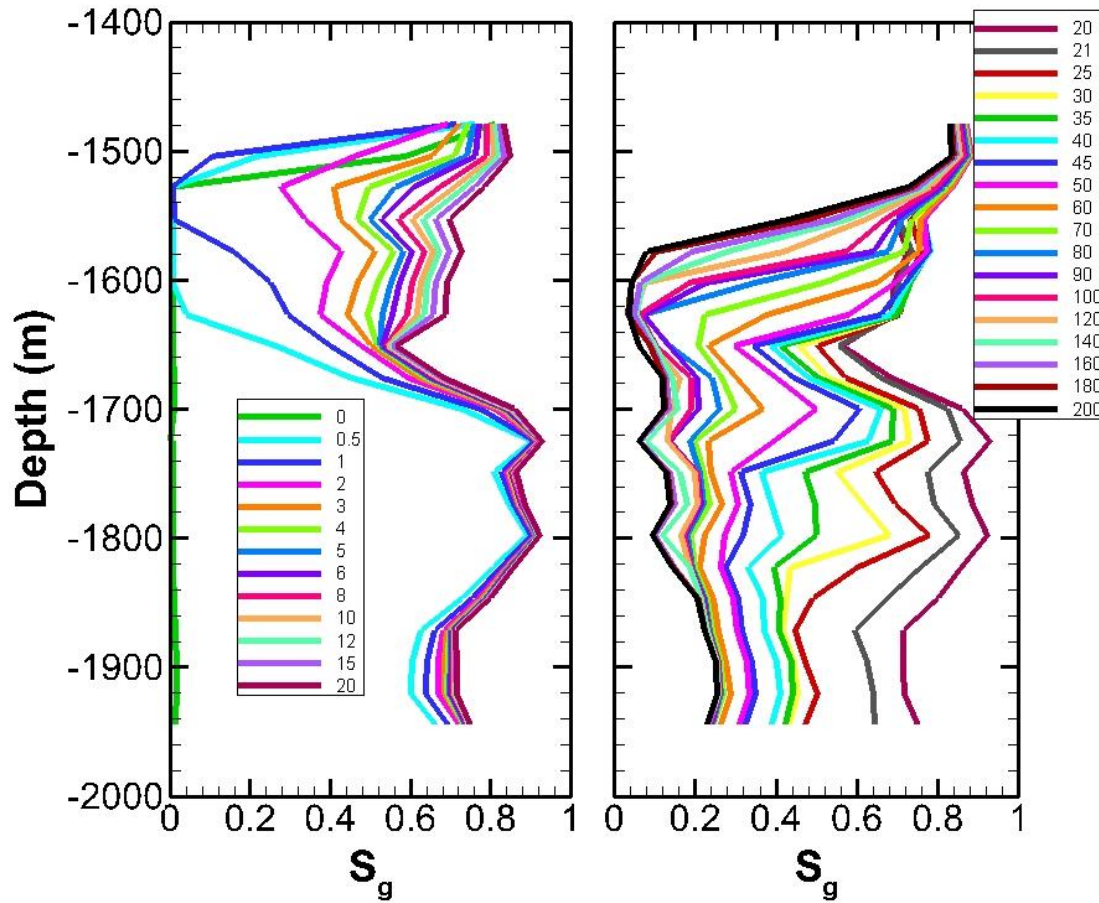


Figure 12. All saturation profiles in the injection well for the actual model. The legend numbers indicate profile time in years. The left-hand-side frame shows times during the injection period and the right-hand-side frame shows times during and beyond the 50-year PISC period. Colors are arbitrarily chosen to enhance profile visibility.

Metrics for comparing models

The two key metrics we use to judge concordance between the actual system and the operational models are (1) the extent of the CO₂ plume updip migration at the end of the 200-year simulation period, denoted R_0 , and (2) the extent of the pressure pulse at the end of the injection period, denoted R_I , as inferred from monitoring well data. Figure 13 shows R_0 as a function of time for the actual model. Each symbol shows the time at which the CO₂ plume arrives at a monitoring well, quantified as a minimum gas saturation of 0.02 and a minimum CO₂ mass fraction of 0.02.

Figure 14 shows the maximum pressure change at the monitoring wells at the end of the injection period, and R_I , taken from Figure 9. The pressure profiles are plotted against distance R from the injection well, and also against $R^{1/2}$. The goal is to use just the points taken from the monitoring wells, and extrapolate to estimate R_I . Plotting dP versus R does not enable a good extrapolation; a polynomial fit yields a very inaccurate estimate of R_I . Plotting dP versus $R^{1/2}$ does much better, allowing a linear fit that yields a reasonable estimate of R_I . This provides a recipe for determining the extent of the pressure pulse for the operating models using only monitoring well data.

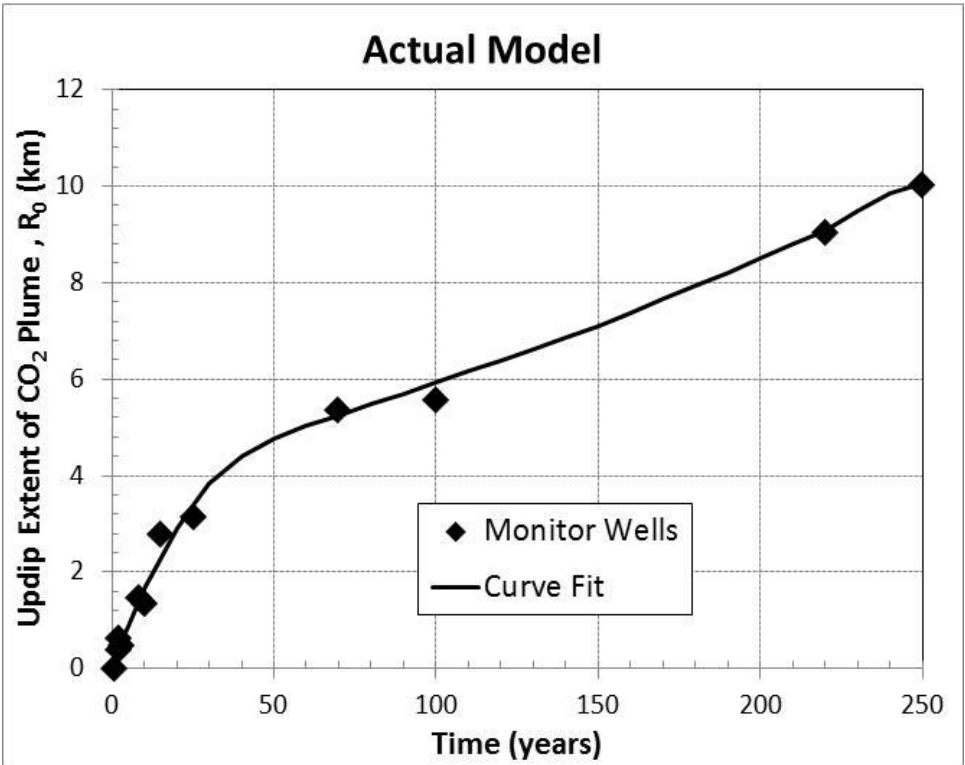


Figure 13. Updip extent of the CO₂ plume, R_0 , for the actual model.

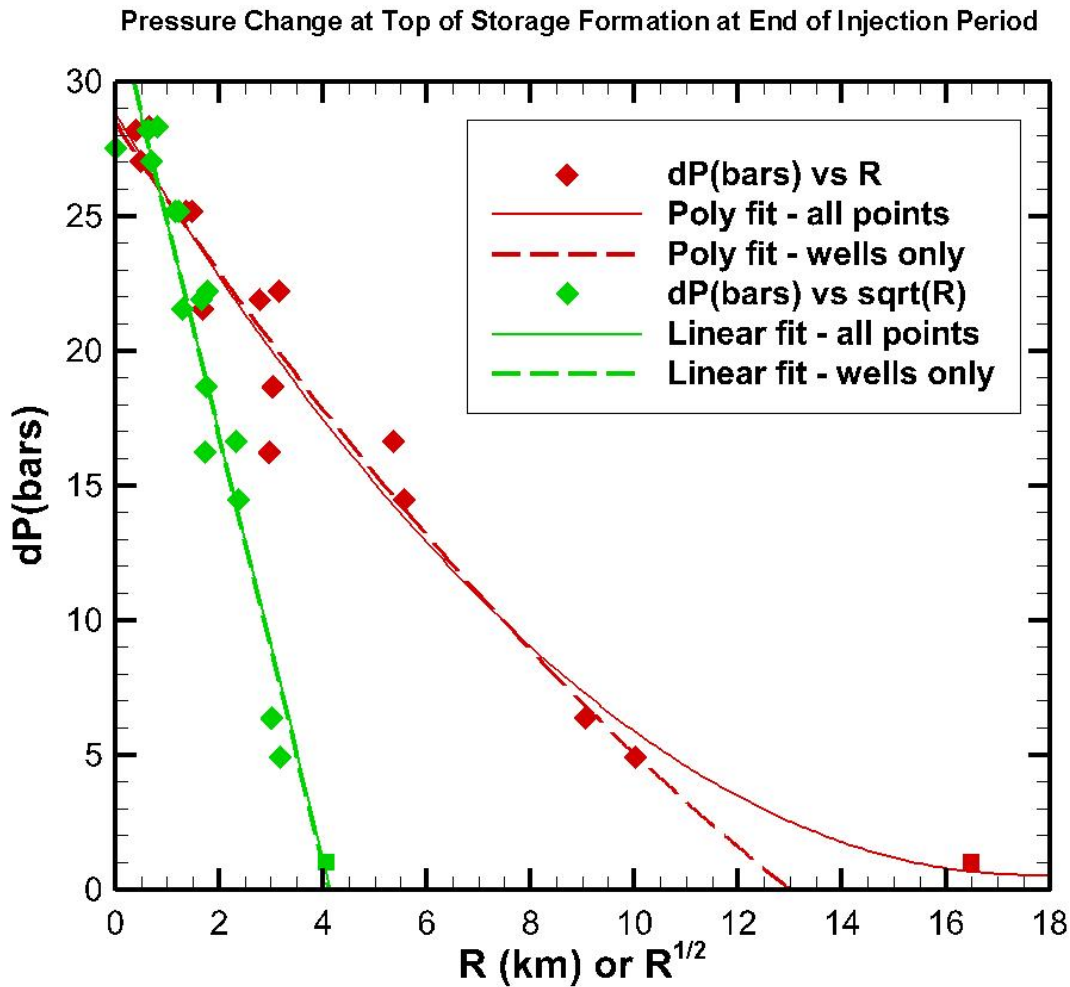


Figure 14. Red diamonds: maximum pressure change at monitoring wells at the end of the injection period, plotted against distance from the injection well, R . Green diamonds: maximum pressure change at monitoring wells plotted against $R^{1/2}$. Squares show $P(R_1) = 1$ bar. The solid lines show best-fit polynomial (red) and linear (green) functions including monitoring well data and $P(R_1)$. The dashed lines show fits including monitoring well data only.

Operational Model Development

Table 2 shows a summary of operational model development. Further details are provided below.

Year 1

The actual model monitoring data for the first year are shown in Figure 15. Note that at one year all but the most distant monitoring wells show a pressure response, but only the injection well shows any change in saturation. At the perforated interval, saturation increase indicates the

344 growing presence of the injected CO₂. Near the top of the formation, the small saturation
345 decrease indicates less CH₄.

346 The corresponding forecast results for the initial operational model are shown in Figure 16. For
347 the operational model, which is homogeneous, the pressure increases for the injection well and
348 nearby monitoring wells are far too large, whereas the pressure changes for more distant
349 monitoring wells tend to be too small. Also, the difference between pressure change at the
350 perforated interval and at the top of the storage formation tends to be too large. Together, these
351 observations suggest that operational-model permeability should be increased. The operational-
352 model saturation profile at the depth of the perforated interval is too uniform, and in particular
353 saturation is too large in the deeper portion of the perforated interval, suggesting that variable-
354 permeability layers should be used. The gradual increase in operational-model saturation above
355 the perforated interval provides information on the vertical permeability there, which seems
356 about right. Because CH₄ is not included in the operational model, the shallow S_g peak observed
357 in the actual model is absent.

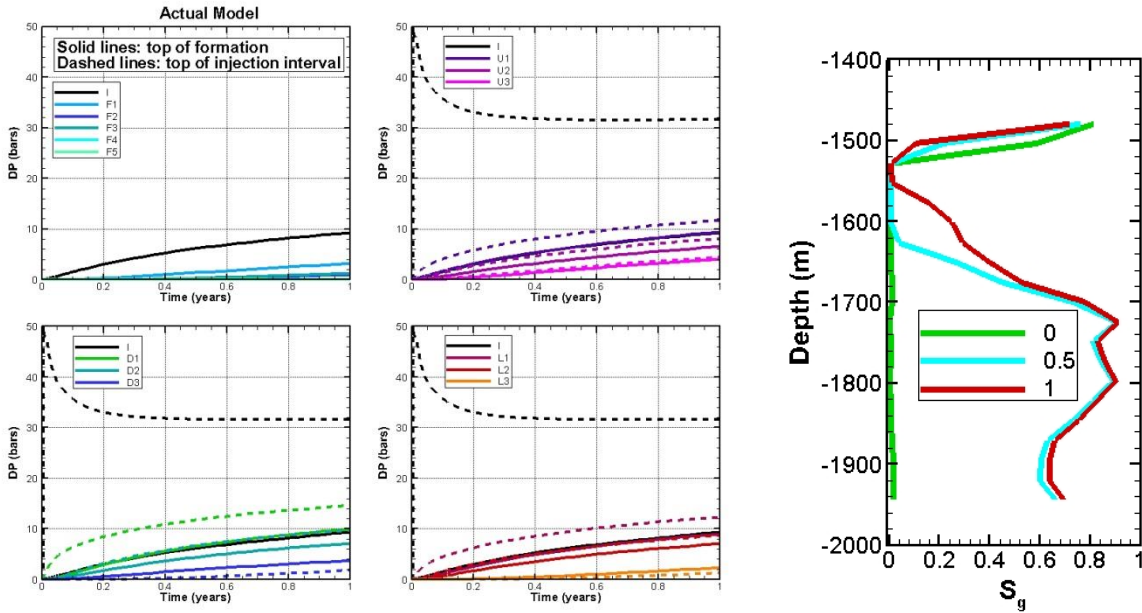


Figure 15. Actual model Year 1 results. (a) pressure transients, (b) saturation profiles at Well I.

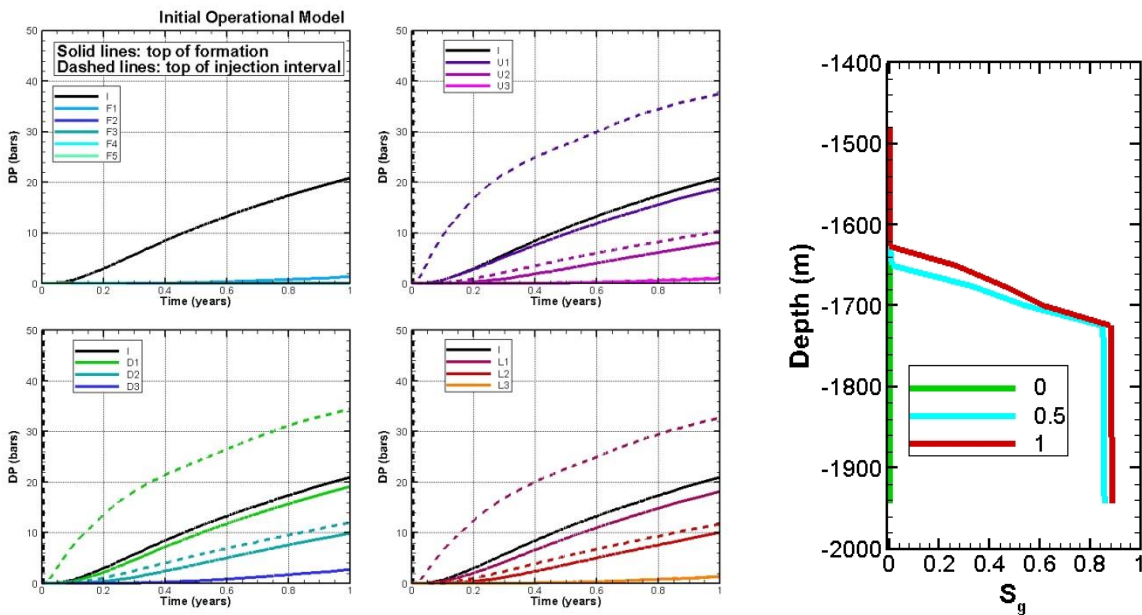


Figure 16. Initial operational model Year 1 forecast: (a) pressure transients, (b) saturation profiles at Well I. The pressure change at the perforated interval in the injection well is off scale at about 100 bars.

After several manual iterative updates of the operational model, including increasing overall permeability and introducing a layered structure at the depth of the perforated interval, the final one-year operational model hindcast results are shown in Figure 17. Horizontal permeability,

which was uniform at 24 mD in the initial operational model, now varies from 3 to 121 mD over the perforated interval and is uniform at 121 mD above the perforated interval. Comparing Figures 15, 16, and 17 indicates that observations after one year allow updates to the operational model properties that greatly improve the pressure and saturation concordance to the actual model compared to the initial operational model, although most operational-model pressure responses are still a few bars too big.

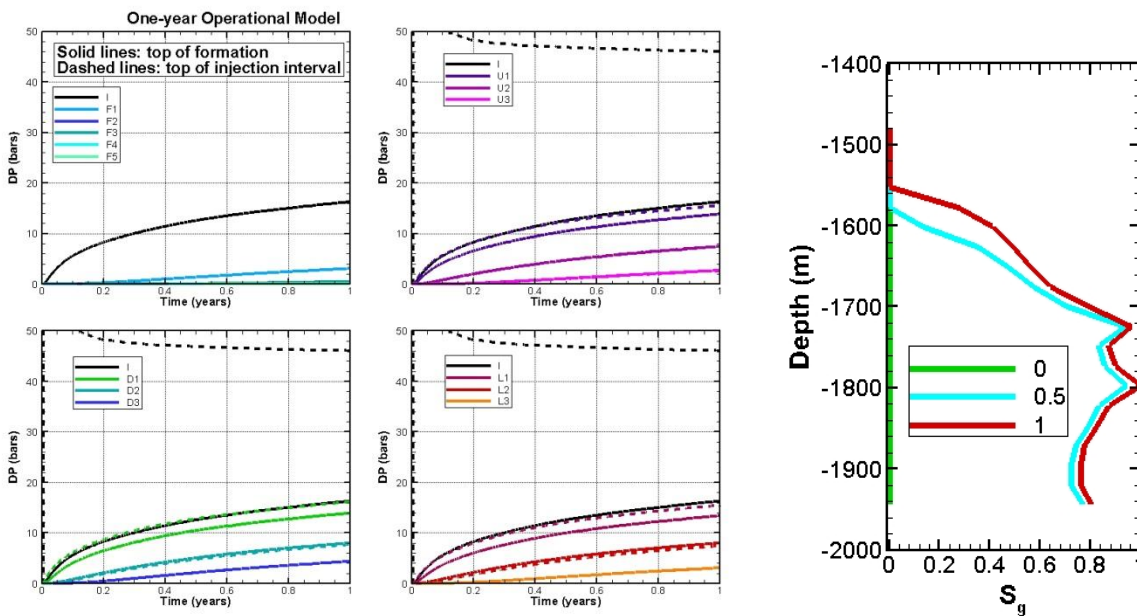


Figure 17. Updated operational model Year 1 hindcast: (a) pressure transients, (b) saturation profiles at Well I.

Year 2

The actual model monitoring data for the second year are shown in Figure 18. At two years the injection well and two nearby monitoring wells show saturation changes relative to initial conditions. The shallowest gas-saturation peak in each well represents attic gas (CH_4). The corresponding forecasts using the updated one-year operational model are shown in Figure 19. For the one-year operational model forecast for two years, the magnitude of the pressure change in the injection well at the perforated interval is significantly too large (~47 bars compared to

~32 bars), but all the other pressure changes are within about 5 bars of the actual model. Note that the actual model shows a bigger separation between pressure response for Well L2 and Well L3 than does the operational model, suggesting that there should be a low-permeability zone separating the two wells. The operational-model saturation response at the perforated interval depth in Wells D1 and L1 is too small, suggesting that the variability of layer permeability should be larger. A small CO₂ peak in the actual-model injection-well saturation profile above the perforated interval suggests that a layered structure is needed for the shallow portion of the storage formation.

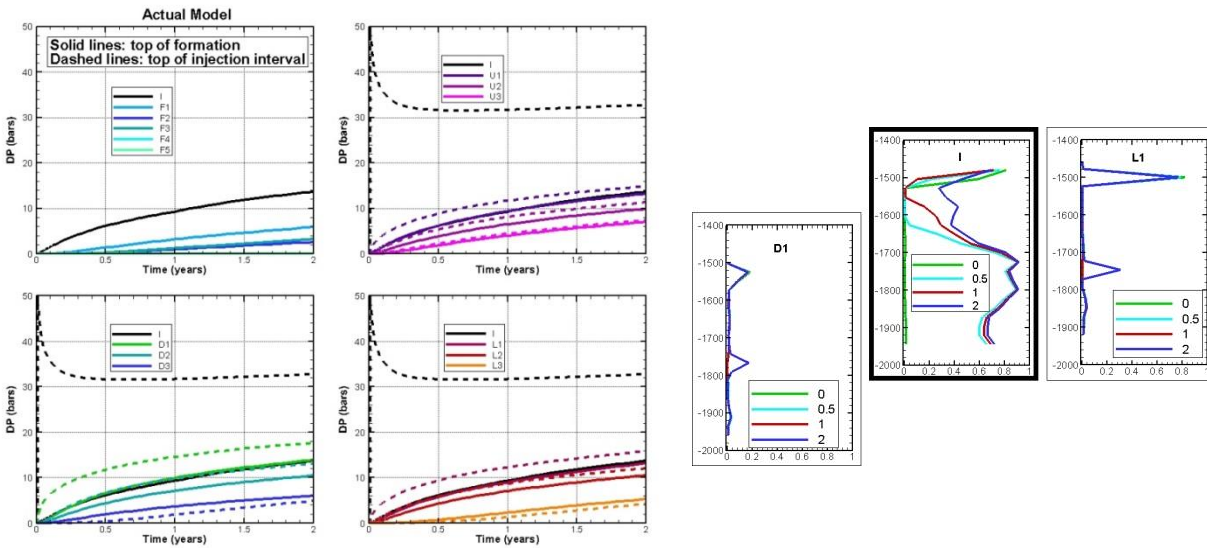


Figure 18. Actual model Year 2 results: (a) pressure transients, (b) saturation profiles.

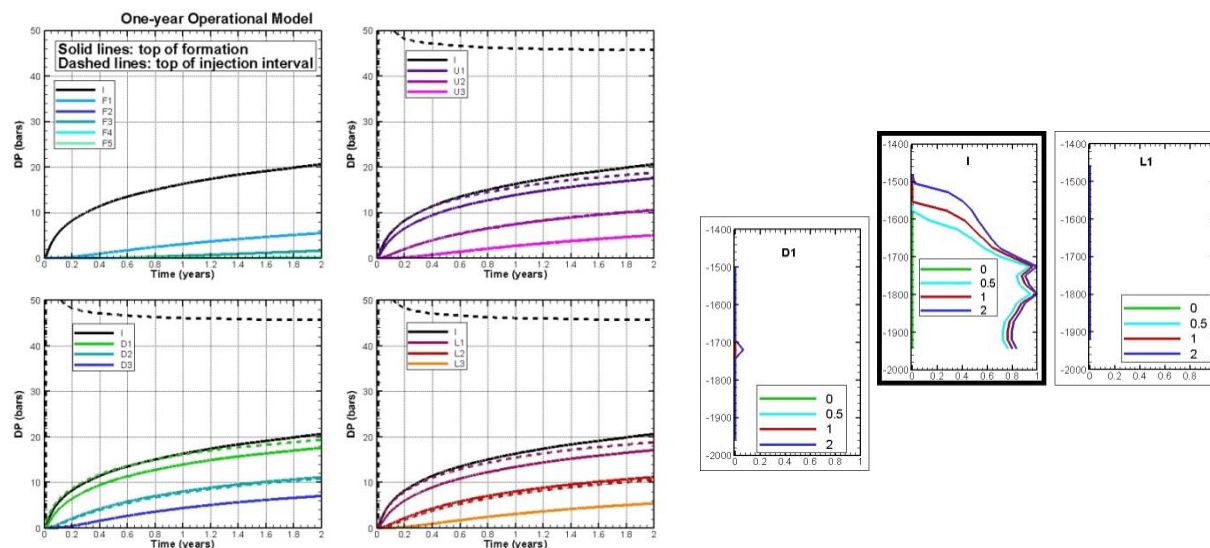


Figure 19. One-year operational model Year 2 forecast: (a) pressure transients, (b) saturation profiles.

After several model updates directed at improving the Year 2 concordance between actual and operational models, we set up a layered structure above the depth of the perforated interval, modified permeabilities at the perforated interval to encourage preferential flow, and introduced a fault between Wells L2 and L3. The final two-year operational model hindcast results are shown in Figure 20. Comparison of Figures 18, 19, and 20 indicates that the two-year operational model generally improves the concordance to the actual model compared to the one-year operational model. In particular, the final pressure change in the injection well at the perforated interval for the operational model is much closer to the actual value (~35 bars compared to ~32 bars), and the difference in pressure response between Wells L2 and L3 is larger, consistent with a low-permeability fault between them. The operational-model S_g peak arrival is still a little late in Wells D1 and L1, and a little early in Well U1, and the CO₂ peak developing above the perforated interval in Well I is not well represented. The shallow CH₄ peaks observed in Wells D1, I, and L1 in the actual model are absent in the operational model.

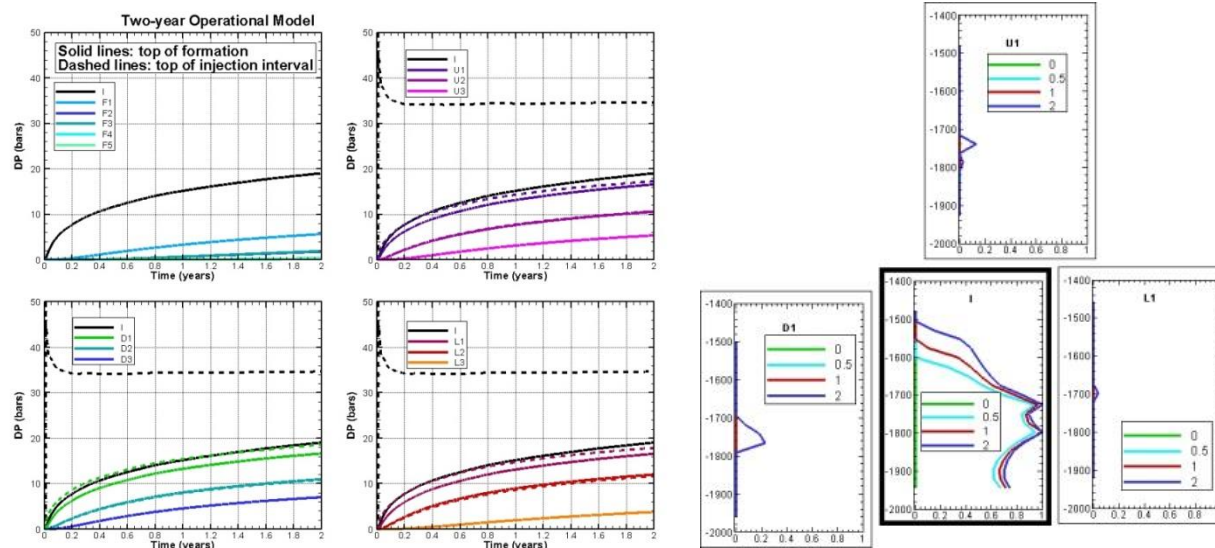


Figure 20. Two-year operational model Year 2 hindcast: (a) pressure transients, (b) saturation profiles.

Year 3

Continuing with the process of comparison of actual to operational models, the actual model monitoring data for the third year are shown in Figure 21. At three years the injection well and three nearby monitoring wells show saturation changes relative to initial conditions. The corresponding forecast results for the two-year operational model are shown in Figure 22. For the operational model, at the injection well and nearby monitoring wells, pressure change is generally a few bars too big. S_g profiles representing CO_2 peaks are generally consistent between the actual and operational models, but the actual peaks are sharper. The shallow CH_4 peaks observed in Wells D1, I, and L1 in the actual model are absent in the operational model.

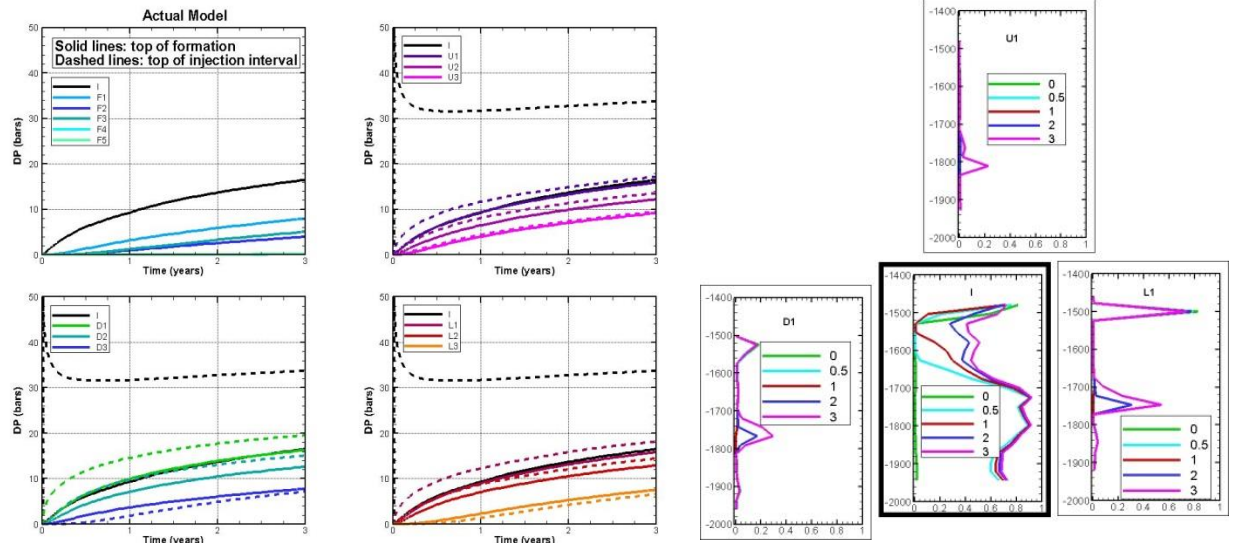


Figure 21. Actual model Year 3 results: (a) pressure transients, (b) saturation profiles.

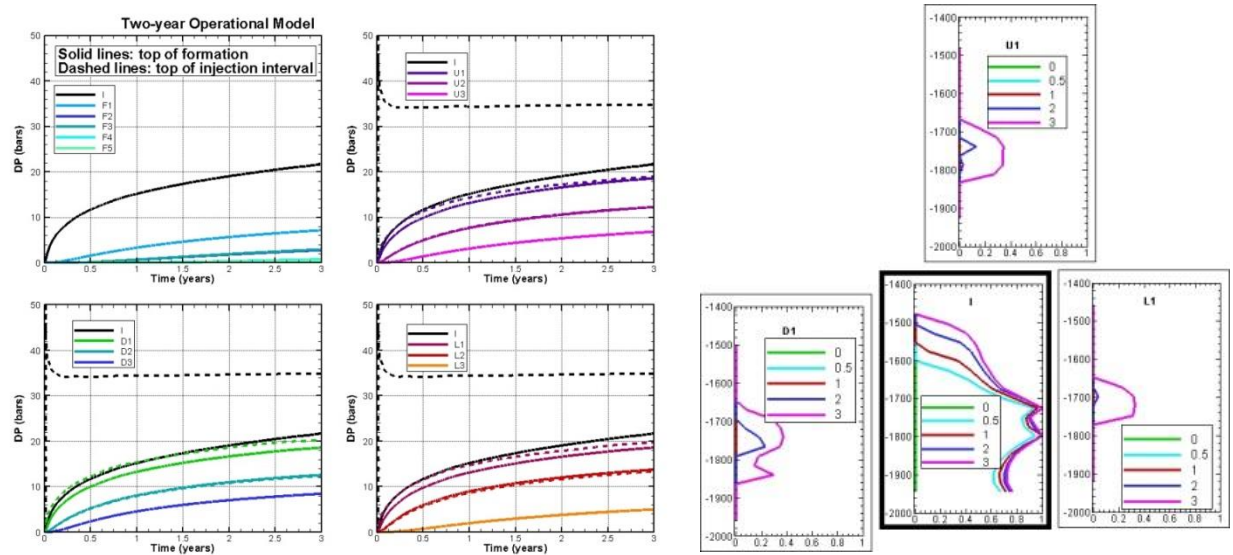


Figure 22. Two-year operational model Year 3 forecast: (a) pressure transients, (b) saturation profiles.

After several operational model updates including doubling the permeability at the depth of the perforated interval, decreasing the permeability of some layers above the depth of the perforated interval, and increasing fault permeability from 5 mD to 15 mD, the final three-year operational

model hindcast results are shown in Figure 23. Comparing Figures 21, 22, and 23 indicates that the three-year operational model somewhat improves the concordance to the actual model compared to the two-year operational model. Compared to the two-year operational model, pressure changes are a little smaller in the injection well (which is now about 5 bars too small at the perforated interval) and nearby monitoring wells (which are now in better agreement with the actual model). Operational-model S_g peaks at nearby monitoring wells are a little bigger, which is generally in better agreement with the actual model. The shallow CH_4 peaks observed in Wells D1, I, and L1 in the actual model are absent in the operational model.

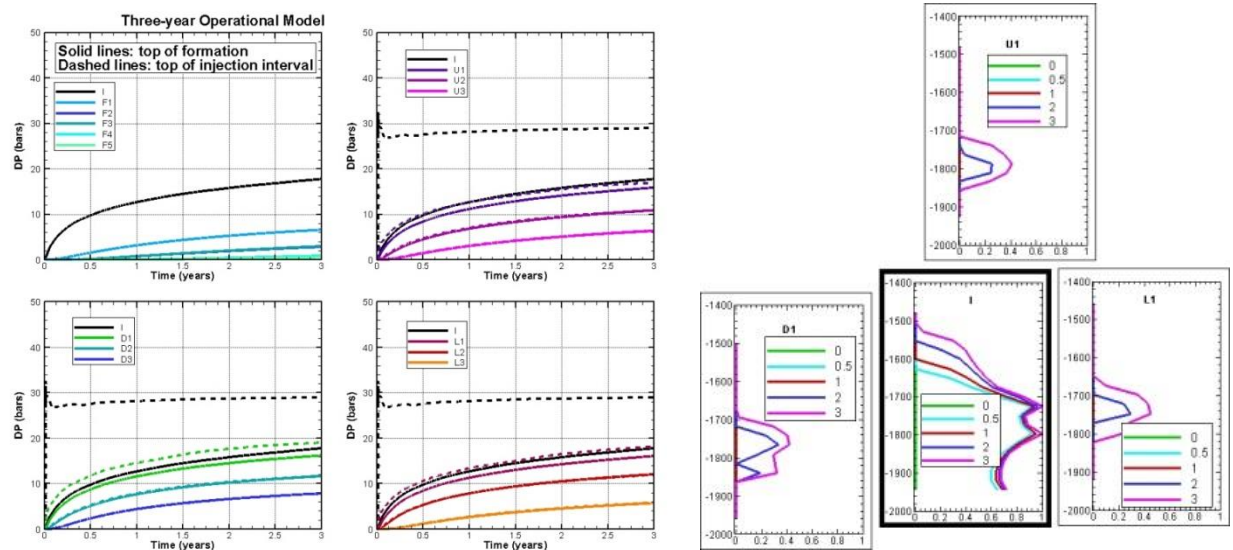


Figure 23. Three-year operational model Year 3 hindcast: (a) pressure transients, (b) saturation profiles.

Year 5

The actual model monitoring data for the fifth year are shown in Figure 24—we skip Year 4 consistent with the idea that the frequency of model updating should decrease as understanding of the system increases. At five years the injection well and three nearby monitoring wells show saturation changes relative to initial conditions. The corresponding forecast results for the three-

year operational model are shown in Figure 25. With a longer time period available for comparing pressure transients, by five years it is apparent that the operational model transients show too much curvature, i.e., they increase too rapidly at first, then level off too much later. After unsuccessful attempts to decrease curvature by increasing storativity by increasing rock compressibility, it was decided that the presence of the additional gas phase in the form of a natural gas cap (CH_4) could provide the additional storativity needed. Thus CH_4 gas was added to the operational model in a pre-injection phase of model development in the same manner as the initial condition of the actual model was developed, i.e., by introducing it uniformly at a low saturation and allowing it to migrate upward into formation attic spaces during an initial gravity equilibration.

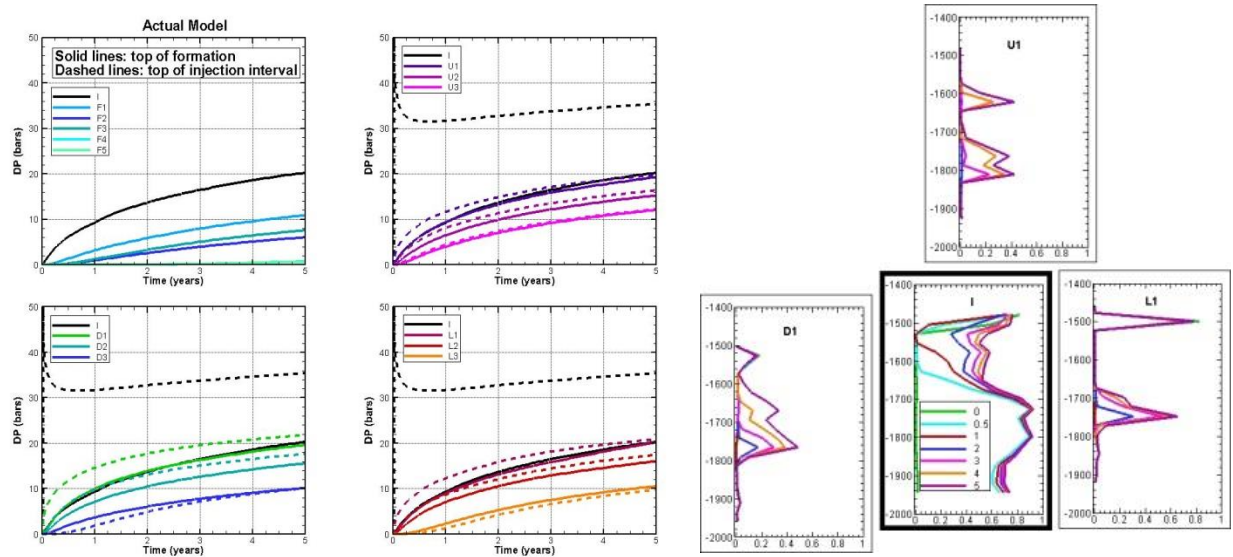


Figure 24. Actual model Year 5 results: (a) pressure transients, (b) saturation profiles.

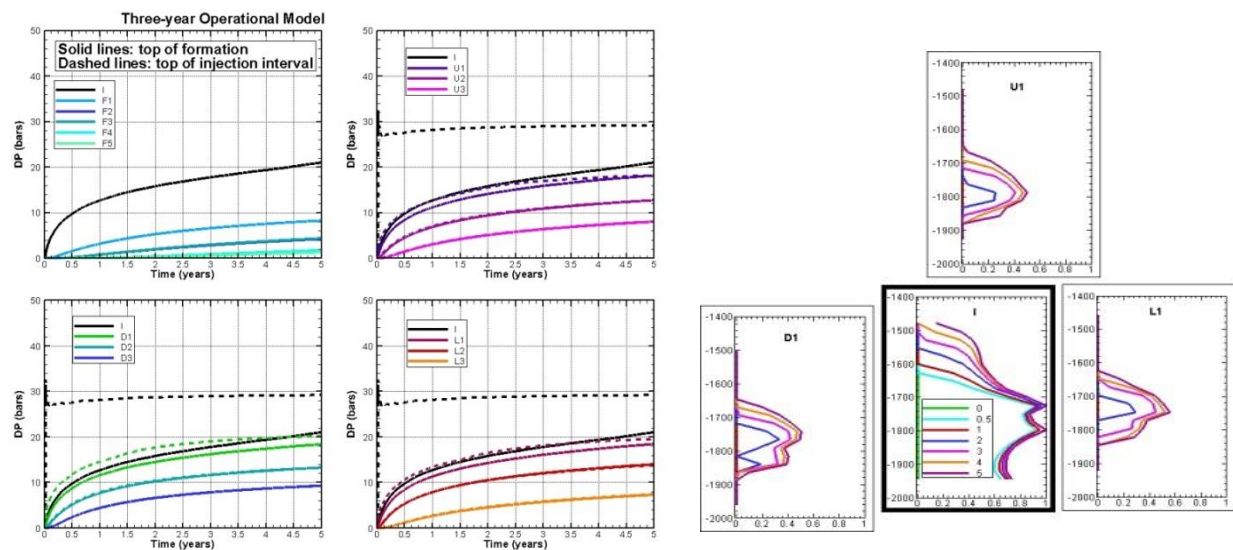


Figure 25. Three-year operational model Year 5 forecast: (a) pressure transients, (b) saturation profiles.

After several model update iterations, the final five-year operational model hindcast results are

shown in Figure 26. The differences from the three-year operational model are the inclusion of

CH₄ in the attic space and a decrease in the permeabilities just above the perforated interval.

Comparing Figures 24, 25, and 26 indicates that the five-year operational model somewhat

improves the concordance to the actual model compared to the three-year operational model.

Compared to the three-year operational model, pressure changes are a little smaller in the

injection well (which is now about 5 bars too small at the perforated interval) and nearby

monitoring wells (which are now in better agreement with the actual model). Overall curvature

of the dP versus time curve is only slightly better than before. Operational-model S_g peaks at

nearby monitoring wells at the depth of the perforated interval, representing injected CO₂, are a

little bigger, which is generally in better agreement with the actual model, and shallow S_g peaks

showing CH₄ are now included.

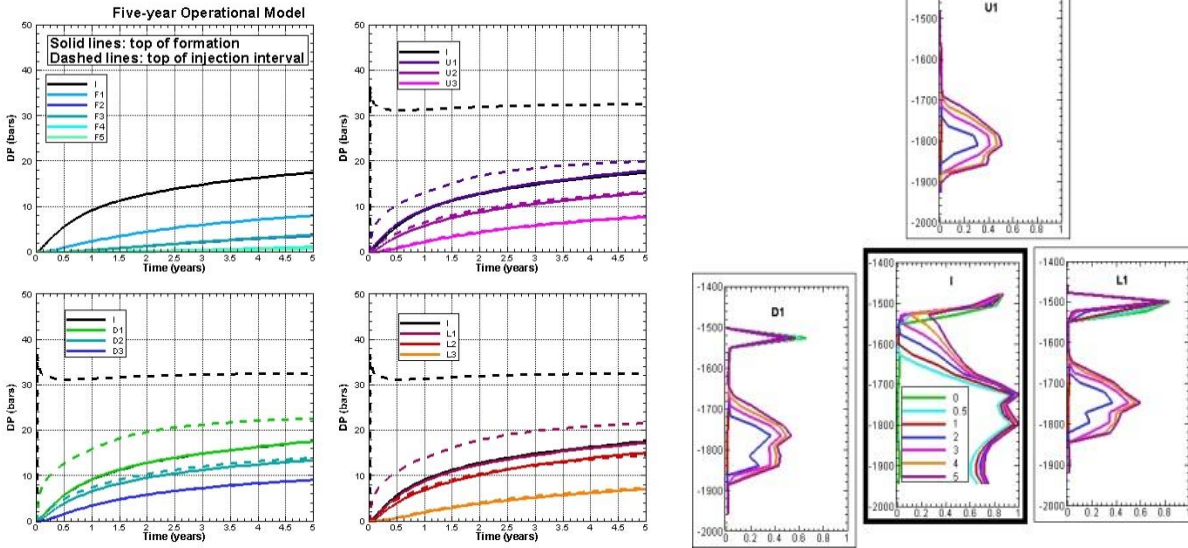


Figure 26. Five-year operational model Year 5 hindcast: (a) pressure transients, (b) saturation profiles.

Year 10

The actual model monitoring data for the tenth year are shown in Figure 27. At ten years the injection well and five nearby monitoring wells show saturation changes relative to initial conditions. The corresponding forecast results for the five-year operational model are shown in Figure 28. For the operational model, the curvature of the dP versus time curve is still too large and most dP values are too small. One possible way to decrease the curvature would be to make the overall flow geometry more linear and less radial, which could be accomplished by placing a low-permeability zone west of the well field. Such a zone should also increase the magnitude of dP at all near-injection monitoring wells. Also, the separation between the Well L2 and Well L3 pressure response curves is too big, suggesting that the L2-L3 fault permeability should be increased. The actual model saturation profiles show several peaks above the perforated interval, representing injected CO_2 that is moving upward through the formation. The operational-model

saturation profiles do not show these peaks, suggesting the need for higher permeabilities in the layers above the perforated interval.

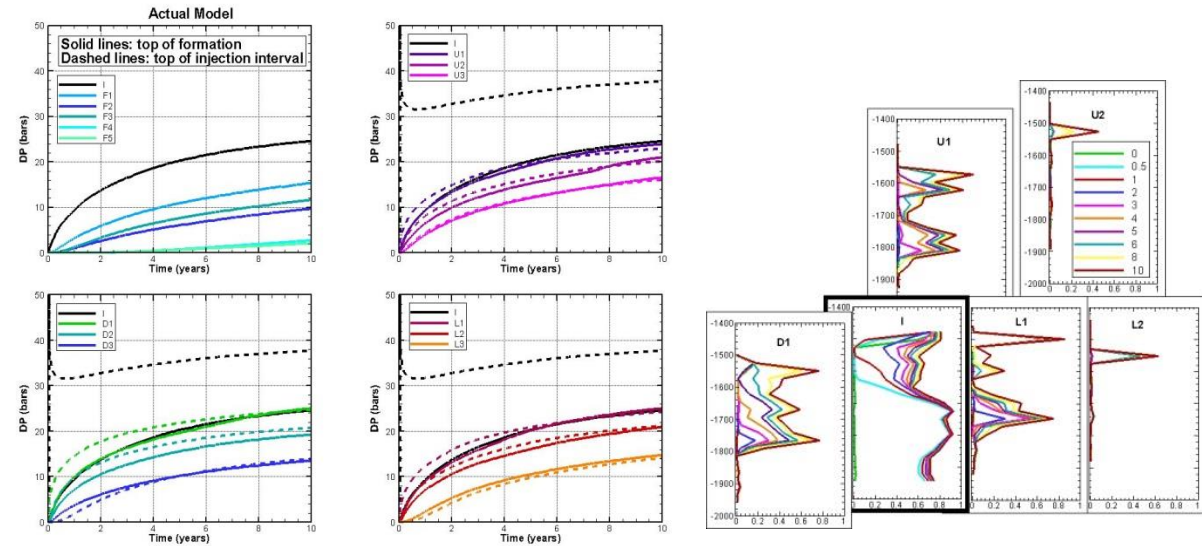


Figure 27. Actual model Year 10 results: (a) pressure transients, (b) saturation profiles.

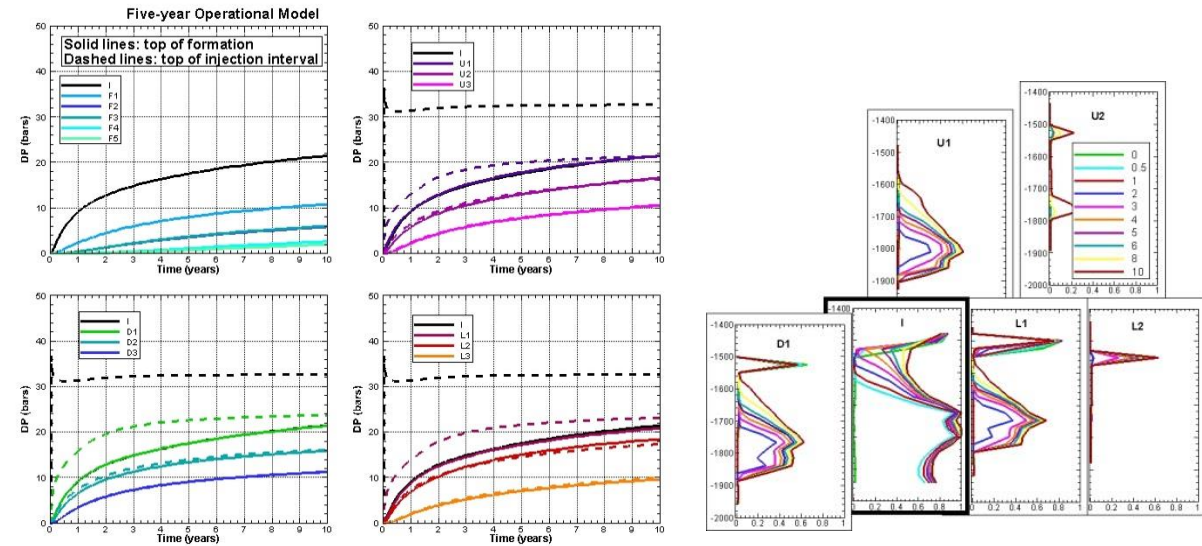


Figure 28. Five-year operational model Year 10 forecast: (a) pressure transients, (b) saturation profiles.

After several operational model update iterations, the final ten-year operational model was updated to include a new fault to the west of the well field with a low permeability of 1 mD, a small increase in the permeabilities just above the perforated interval with a corresponding small decrease in the permeabilities at the perforated interval, and an increase in the L2-L3 fault permeability from 15 to 30 mD. The final ten-year operational model hindcast results are shown in Figure 29. Comparing Figures 27, 28, and 29 indicates that the ten-year operational model somewhat improves the concordance to the actual model compared to the five-year operational model. Compared to the five-year operational model, pressure changes are a little bigger in the injection well and nearby monitoring wells (which are now in better agreement with the actual model). The separation between Well L2 and Well L3 pressure curves is slightly smaller. The overall curvature of the dP versus time curve is only slightly better than before. Operational-model S_g peaks at nearby monitoring wells at depths above the perforated interval, representing injected CO_2 , are a little bigger, which is generally in better agreement with the actual model.

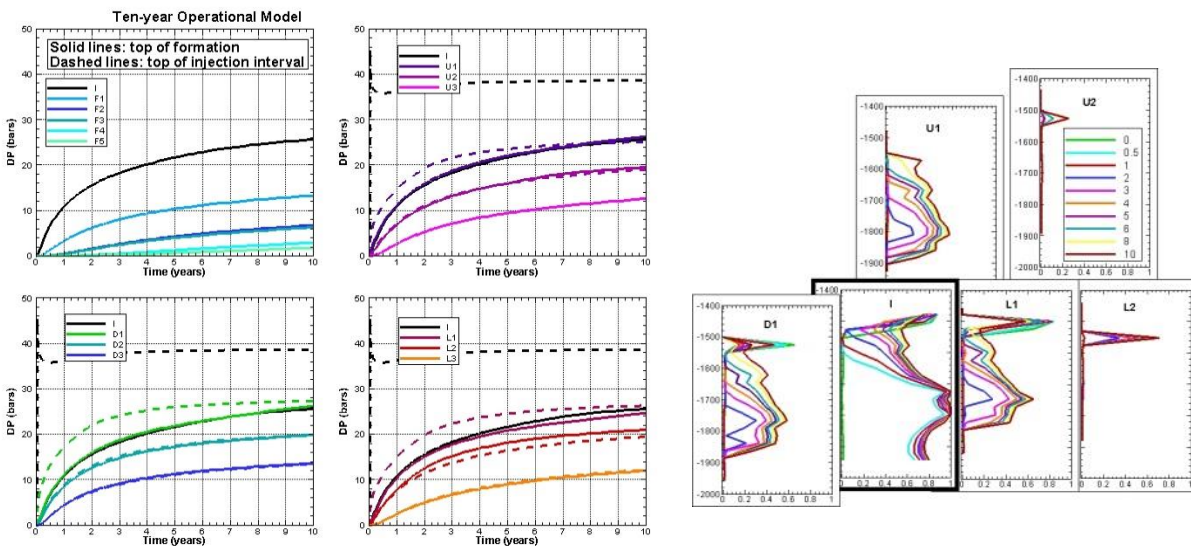


Figure 29. Ten-year operational model Year 10 hindcast: (a) pressure transients, (b) saturation profiles.

518

519 ***Year 20 – End of Injection Period***

520 The actual model monitoring data for the 20th year are shown in Figure 30. At 20 years the
521 injection well and six monitoring wells show saturation changes relative to initial conditions. The
522 corresponding forecast results for the ten-year operational model run out to 20 years are shown
523 in Figure 31. For the actual model all dP versus time curves are gradually increasing, but for the
524 operational model they tend to increase too fast early, then level off too much late, showing too
525 much curvature. This occurs more for the pressures at the depth of the perforated interval and is
526 especially obvious at the injection well. However, the magnitude of dP is about right at 20 years.
527 In an attempt to get more gradually increasing pressure curves, the two faults were extended
528 farther updip, to create a more linear, less radial flow geometry. This is the only change made to
529 create the final twenty-year operational model, and hindcast results are shown in Figure 32. The
530 dP versus time curves show slightly less curvature. The saturation profiles for the ten-year and
531 twenty-year operational models are very similar, and provide a reasonable concordance to the
532 actual model.

533

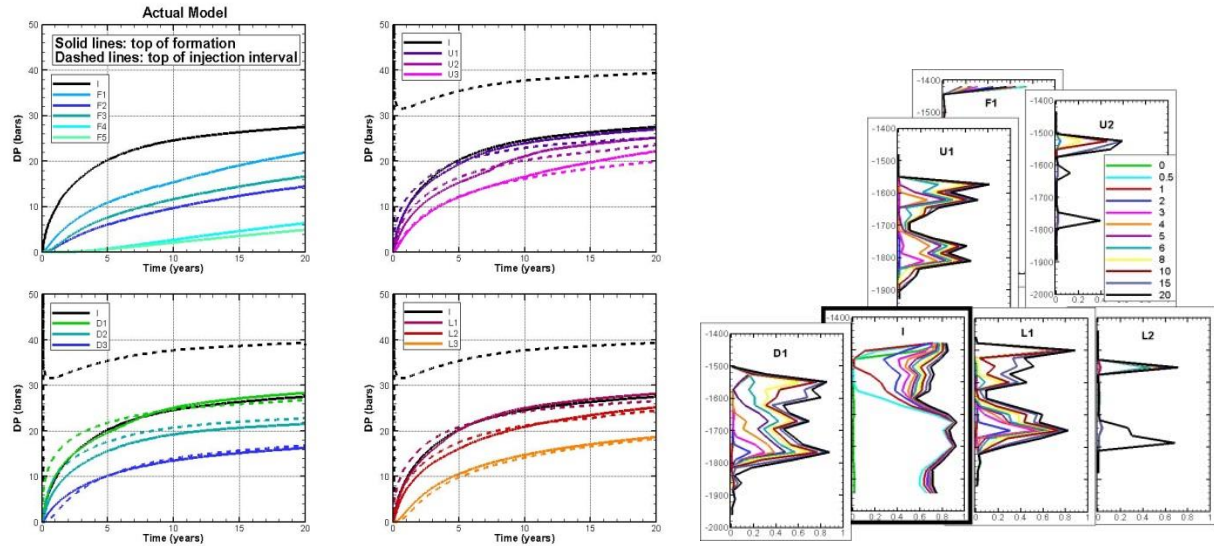


Figure 30. Actual model Year 20 results: (a) pressure transients, (b) saturation profiles.

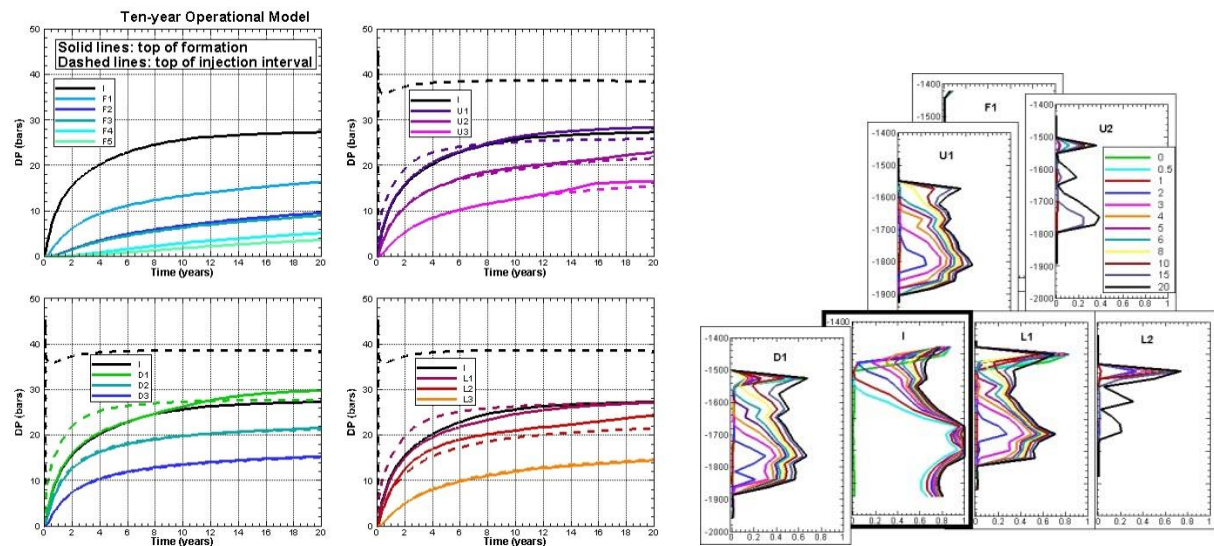


Figure 31. Ten-year operational model Year 20 forecast: (a) pressure transients, (b) saturation profiles.

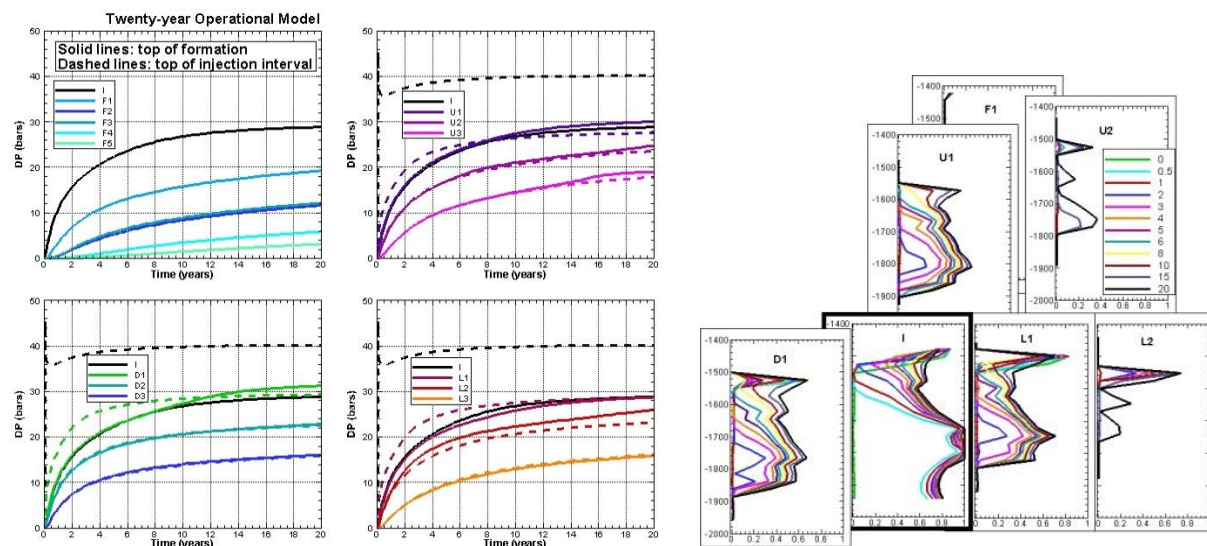


Figure 32. Twenty-year operational model Year 20 hindcast: (a) pressure transients, (b) saturation profiles.

Year 25

The actual model monitoring data for the 25th year are shown in Figure 33. This is the first observation within the post-injection period. For clarity, only saturation profiles from the post-injection period are shown. After injection ends at 20 years, pressure change is decreasing in all wells except the two most distant monitoring wells, F4 and F5, where it is still increasing slowly. At 25 years the injection well and seven monitoring wells show saturation changes relative to initial conditions. Gas saturation is decreasing in the deeper portion of the formation and increasing in the shallow portion, as buoyancy flow acts to lift the CO₂ plume. The corresponding forecast results for the twenty-year operational model are shown in Figure 34. This is a non-hysteretic model with $S_{gr} = 0$ during the injection period and $S_{gr} = 0.2$ during the post-injection period.

By the end of the injection period, most of the dP values for the twenty-year operational model are too big, and the curvature of the dP versus time curve indicates too rapid a response for all

557 wells, which is notable especially at the perforated interval of Well I, which flattens out too
558 much towards the end of the injection period, and the far wells F4 and F5, for which dP does not
559 continue to increase after injection ends. This suggests that the rock compressibility should be
560 larger, to provide a generally slower response. Comparing the post-injection saturation profiles
561 for the actual and twenty-year operational model shows that the gradual decline in gas saturation
562 over the lower half of the reservoir, which occurs as CO₂ moves upward under buoyancy forces
563 and water imbibes back into the pore space, is not produced by the operational model, indicating
564 that this non-hysteretic approximation with $S_{gr} = 0.2$ for the post-injection period overestimates
565 trapping of CO₂. After several iterations, the final twenty-five year operational model has
566 doubled rock compressibility ($0.3\text{E-}8 \text{ Pa}^{-1}$ to $0.6\text{E-}8 \text{ Pa}^{-1}$), and two variations considered to better
567 represent imbibition: a non-hysteretic model with $S_{gr} = 0$ for the post-injection period and a
568 hysteretic model. The hysteretic model has a variable S_{gr} ; during the injection period it remains
569 zero nearly everywhere, and during the post-injection period it varies spatially and temporally
570 from zero to $S_{grmax} = 0.2$, depending on the maximum value of S_g experienced by a given
571 location. At the perforated interval, where the maximum S_g during the injection period was near
572 one, $S_{gr} \sim S_{grmax}$.

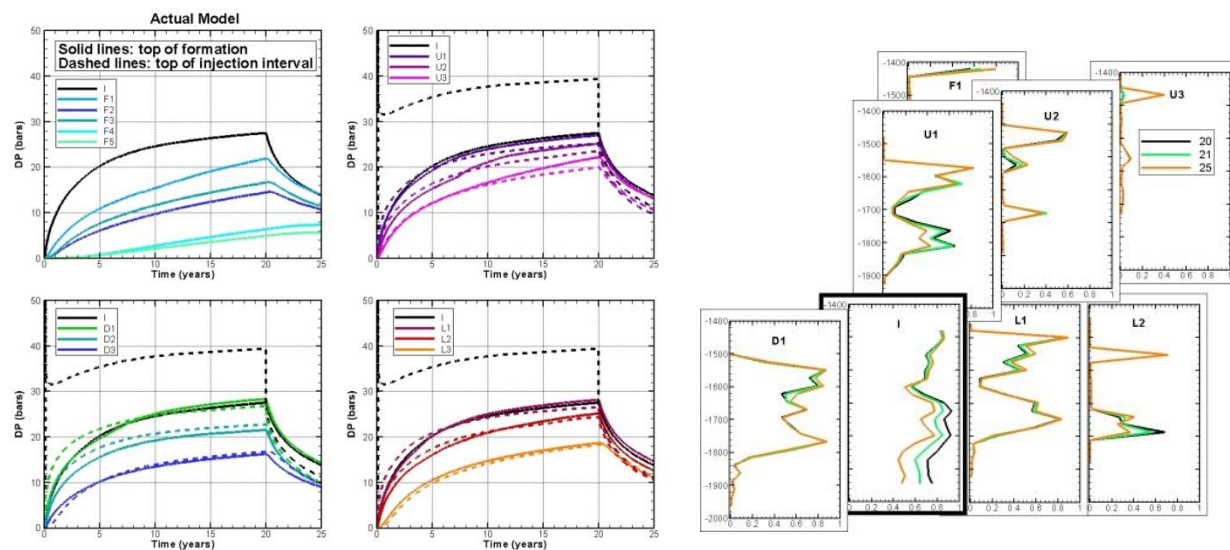


Figure 33. Actual model Year 25 results: (a) pressure transients, (b) saturation profiles for the first five years of the post-injection period.

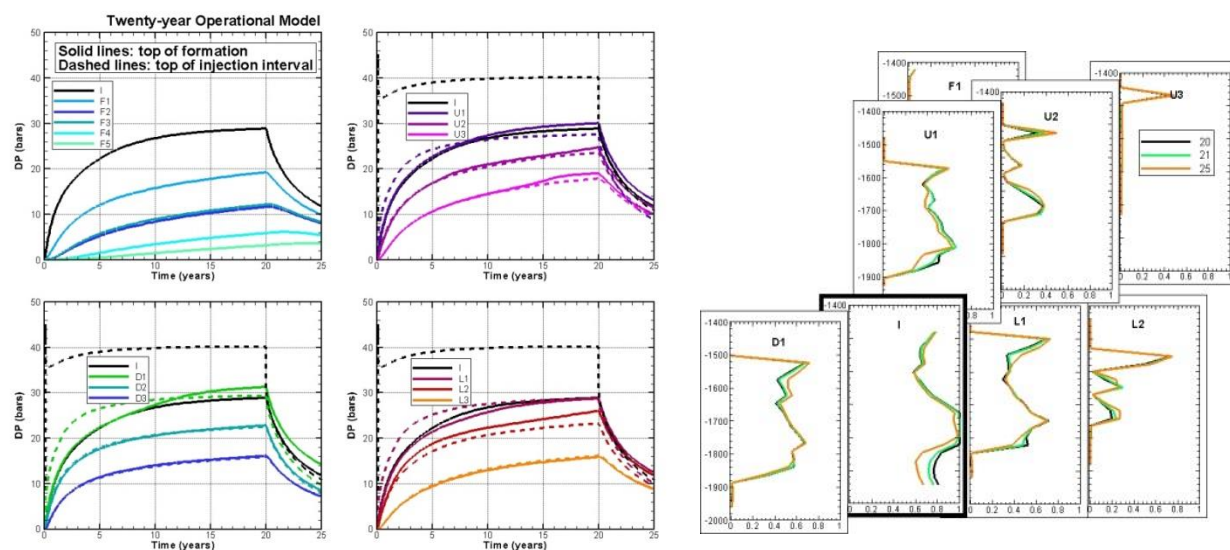
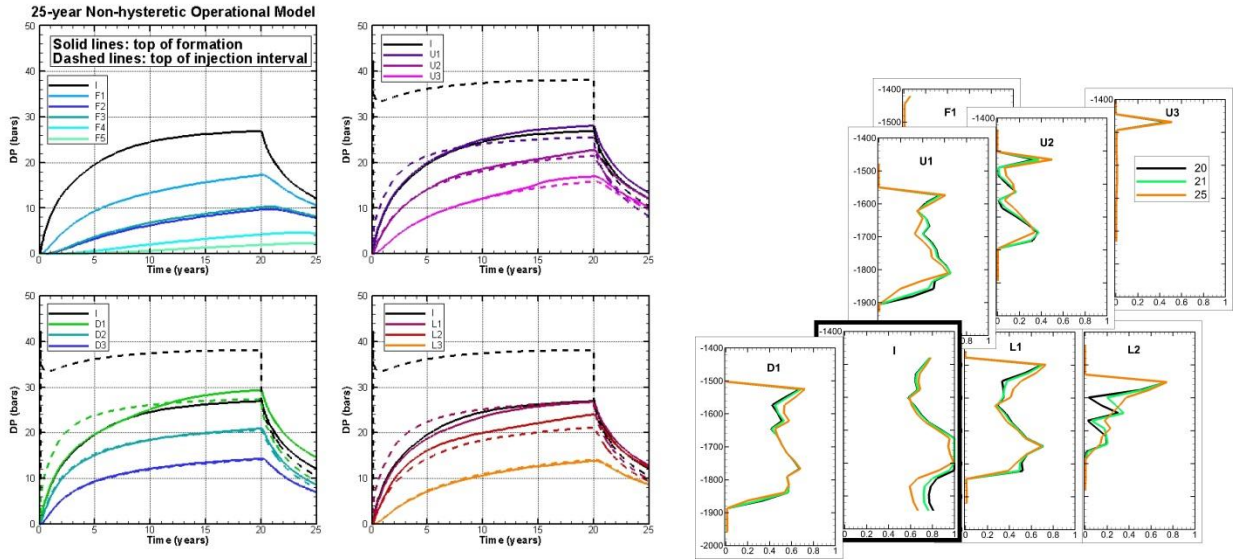


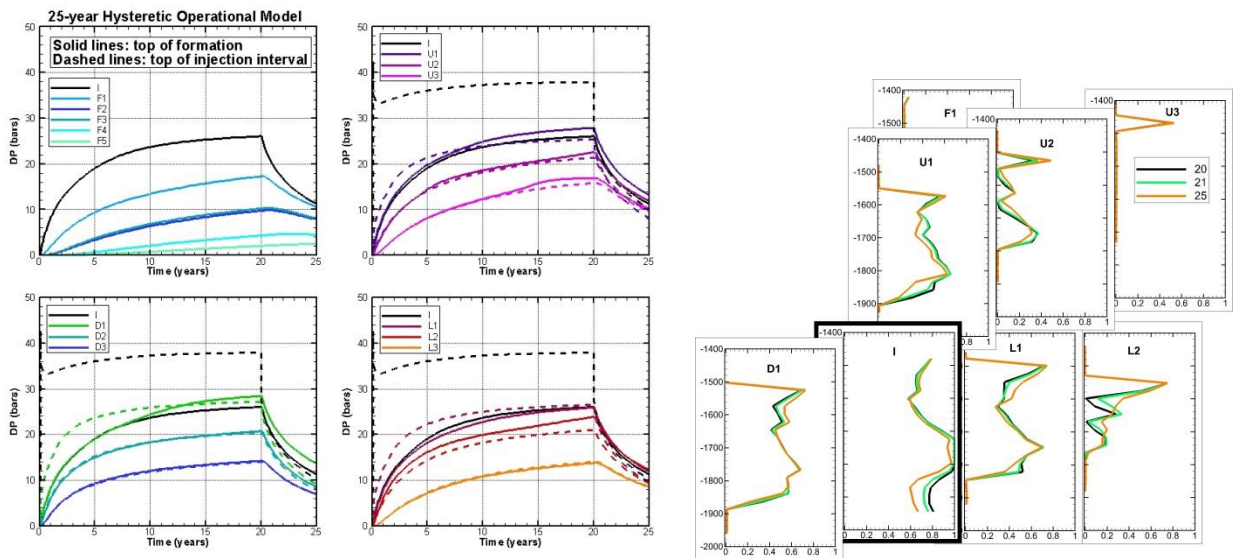
Figure 34. Twenty-year operational model Year 25 forecast: (a) pressure transients, (b) saturation profiles for the first five years of the post-injection period. Non-hysteretic model with $S_{gr} = 0.2$ during post-injection period.

The hindcast results for the non-hysteretic twenty-five-year operational model (Figure 35) and hysteretic twenty-five-year operational model (Figure 36) show similar pressure transients and saturation profiles. Although the maximum pressure change at the end of injection is now

584 slightly small for most wells, the curvature of the dP versus time curve is a little better.
 585 Operational-model saturation profiles now match the character of the actual model much better,
 586 with gradual saturation decline in the lower half of the reservoir.



587
 588 *Figure 35. Twenty-five-year non-hysteretic model Year 25 hindcast: (a) pressure transients, (b)*
 589 *saturation profiles for the first five years of the post-injection period. Non-hysteretic model with*
 590 *$S_{gr} = 0$ during post-injection period.*



591
 592 *Figure 36. Twenty-five-year hysteretic model Year 25 hindcast: (a) pressure transients, (b)*
 593 *saturation profiles for the first five years of the post-injection period.*

Year 50

The actual model monitoring data for the 50th year are shown in Figure 37. At 50 years the injection well and seven monitoring wells show saturation changes relative to initial conditions. Pressure change is now decreasing in all wells. Gas saturation continues decreasing in the deeper portion of the formation and increasing in the shallow portion, as buoyancy flow acts to lift the CO₂ plume upward and updip in the storage formation. The corresponding forecast results for the saturation profiles for the twenty-five-year operational models are shown in Figure 38. Pressure transients for the operational models (not shown) are similar to those for the actual model.

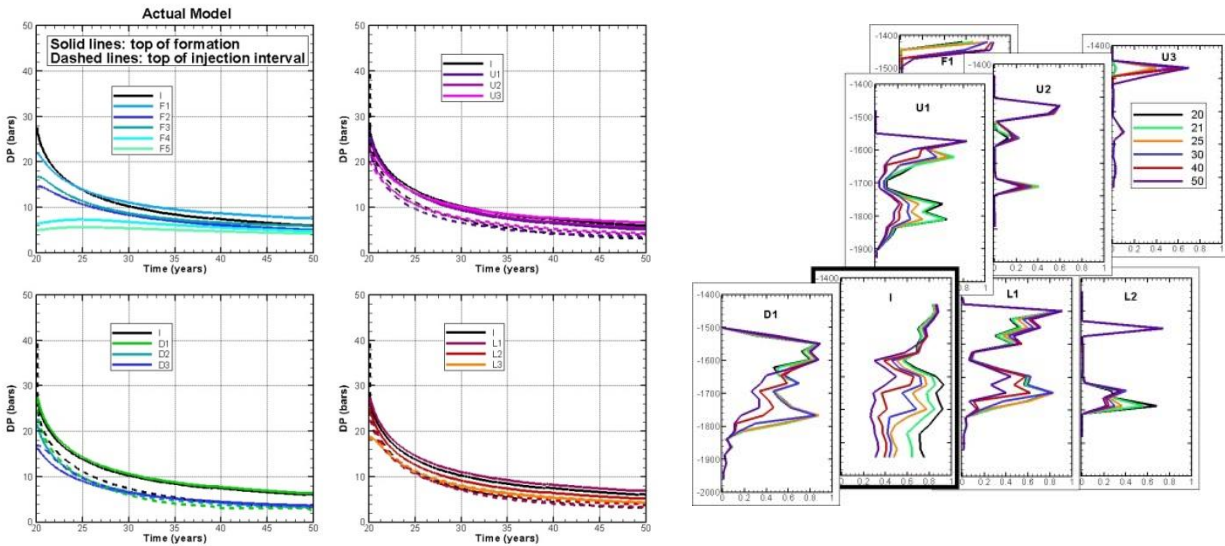


Figure 37. Actual model Year 50 results: (a) pressure transients, (b) saturation profiles for the first 30 years of the post-injection period.

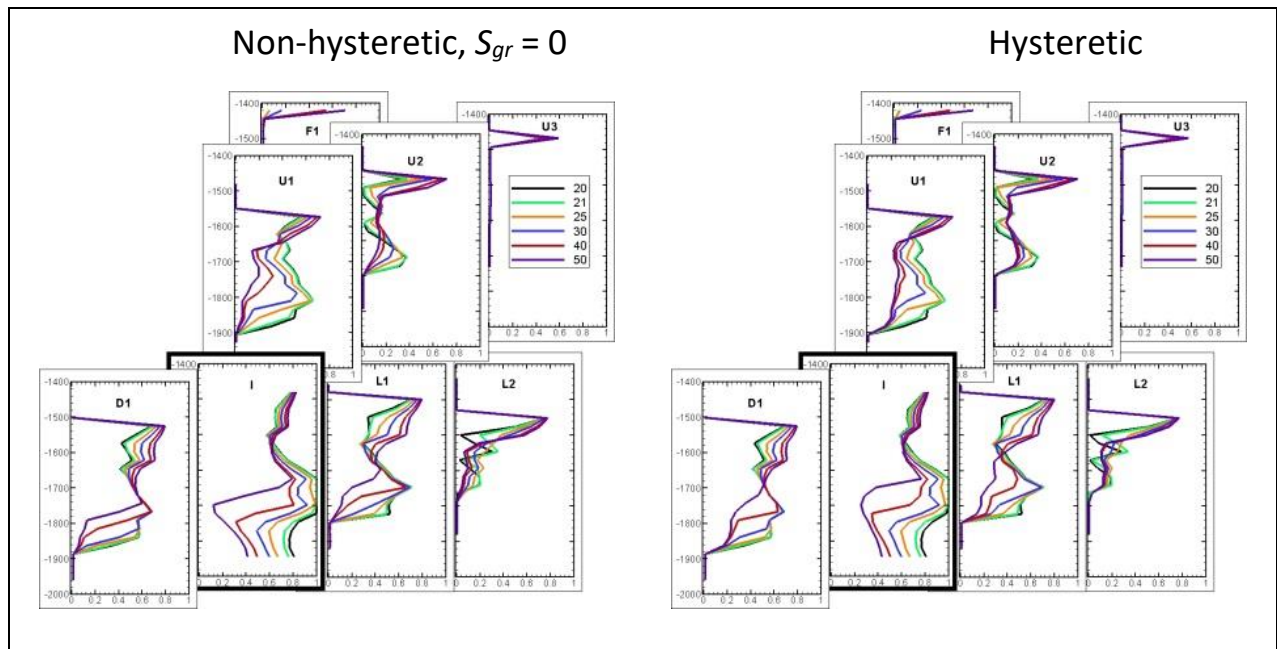


Figure 38. Twenty-five-year operational models Year 50 forecast: saturation profiles for the first 30 years of the post-injection period.

Comparison of the late-time saturation profiles in Figure 38 indicates that as S_g decreases, the non-hysteretic model fails to show a convergence of S_g to 0.2 as the actual model (Figure 37) and hysteretic operational model do. Hence only the hysteretic model is used for continued operational model development.

Years 100, 150, and 200

The actual model monitoring data through the end of the PISC period at 70 years and on to 200 years are shown in Figure 39. Starting at 100 years, the injection well and nine monitoring wells show saturation changes. The corresponding forecast results for the fifty-year operational model are shown in Figure 40. The gradual decline in the dP versus time curves is similar in both models, but the actual model dP curves tend to plateau above zero, whereas most of the operational model curves approach zero. Both models show the saturation continuing to decline in the lower half of the formation, but at a slowing rate, as saturations approach residual

saturation. The fifty-year operational model concordance to the actual data is deemed acceptable for 100, 150, and 200 years and no further model development is done.

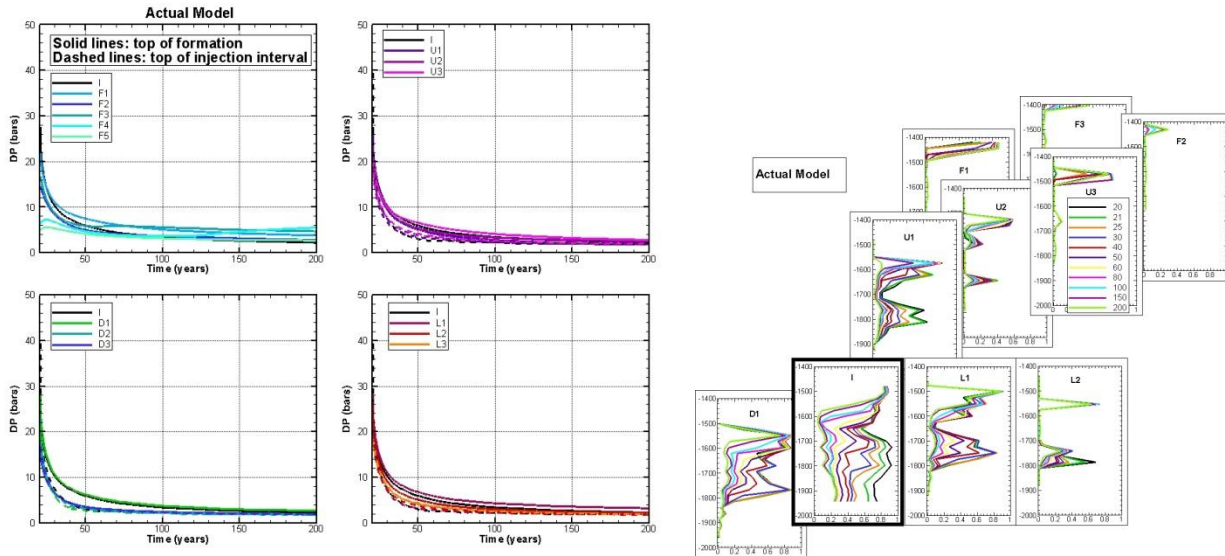


Figure 39. Actual model pressure transients and saturation profiles for the entire post-injection simulation period.

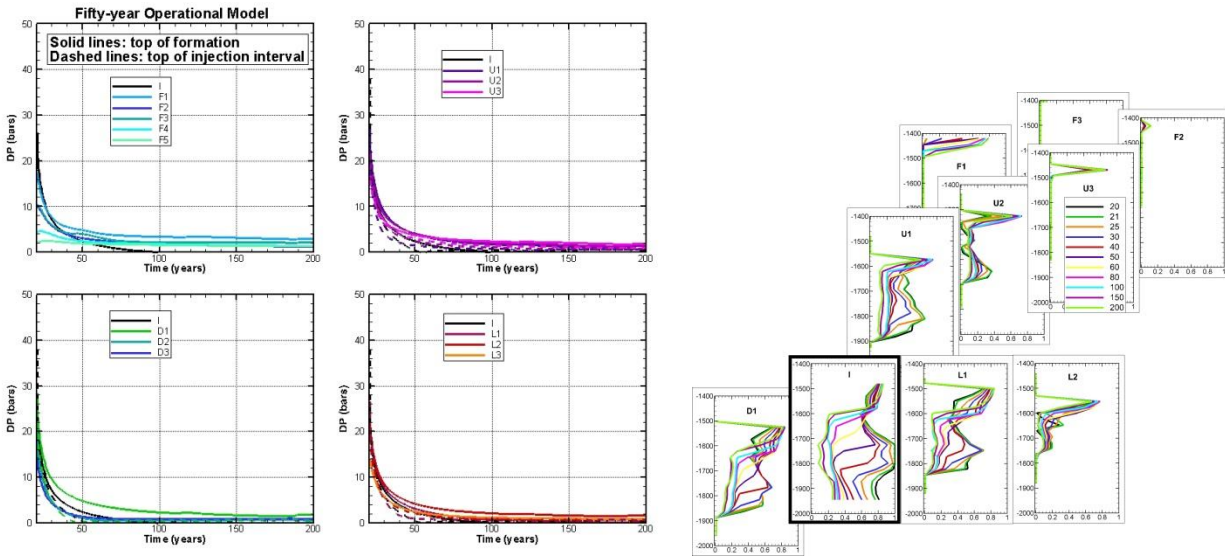


Figure 40. Fifty-year operational model pressure transients and saturation profiles for the entire post-injection simulation period.

629 Table 2. Summary of development of operational models.

Year	Change in Saturation Profile*	Operational Model at Start of Year's Development	Observations from Operational Model		Changes Made to Operational Model	Number of Iterations
			Pressure transients	Saturation profiles		
1	I	Permeability 24 mD, no layering, no faults, no lateral heterogeneity, non-hysteretic relative permeability, no CH ₄	dP too big near I, too small far from I	$S_g(z)$ too uniform at I	Increase permeability; introduce layering at perforated interval	6
2	I, L1, D1	Layering at perforated interval (3 - 121 mD), permeability 121 mD above perforated interval	dP at I perforated interval too big; dP at L3 too big	S_g peaks at L1 and D1 late arriving; S_g peak above perforated interval in I is missing	Modify permeability layering at perforated interval; introduce layering above perforated interval; Introduce fault between L2 and L3	3
3	I, L1, D1, U1	Layering at perforated interval (2 mD – 300 mD), layering above perforated interval (100 – 150 mD), L2/L3 fault permeability 5 mD	dP too big near I	S_g peaks okay, but too broad	Modify permeability layering; increase permeability at perforated interval, decrease permeability shallow	3
5	I, L1, D1, U1	Layering at perforated interval (4 mD – 600 mD), layering above perforated interval (50 – 150 mD), fault	Curvature of P vs t too large; dP at I perforated interval	S_g peaks okay, but too broad	Modify permeability layering: decrease permeability just above perforated interval; include	8

		permeability 15 mD	too small		CH ₄	
10	I, L1, L2, D1, U1, U2	Layering at perforated interval (4 mD – 600 mD), layering above perforated interval (25 – 141 mD), fault permeability 15 mD; CH ₄ included	dP generally too small; curvature unchanged	S_g peaks at perforated interval okay, shallow CO ₂ peaks too small	Modify permeability layering: decrease permeability at perforated interval and increase permeability shallow; Introduce fault west of well field; increase permeability of L2/L3 fault	6
20	I, L1, L2, D1, U1, U2, F1	Layering at perforated interval (3 mD – 400 mD), layering above perforated interval (50– 500 mD), L2/L3 fault permeability 30 mD; west fault permeability 1 mD; CH ₄ included	Curvature a little smaller, but still too large; dP generally okay at 20 years	S_g profiles generally good for both CO ₂ and CH ₄	Extend both faults farther updip	1
25	I, L1, L2, D1, U1, U2, U3, F1	Same as 20 years except faults extended in updip direction. Non-hysteretic model with $S_{gr} = 0.2$ during post-injection period	Curvature a little smaller	S_g profiles do not decrease enough from their maximum during early post-injection period	Double rock compressibility; eliminate non-hysteretic model with $S_{gr} = 0.2$ during post-injection period; develop non-hysteretic model with $S_{gr} = 0$ during post-injection period and hysteretic model with $S_{grmax} = 0.2$	3

50	I, L1, L2, D1, U1, U2, U3, F1	Same as 25 years except rock compressibility doubled to 0.6e-8; non-hysteretic model with $S_{gr} = 0$, hysteretic model with $S_{grmax} = 0.2$	Curvature a little smaller; dP still too small at far wells; no significant effect of hysteresis	Non-hysteretic model with $S_{gr} = 0$: S_g profiles decrease too much near $S_g = 0.2$	Eliminate non-hysteretic model with $S_{gr} = 0$	2
100	I, L1, L2, D1, U1, U2, U3, F1, F2, F3	Same as 50 years, but hysteretic model only	dP all approaching zero	S_g changes getting smaller		1

630 *Bold indicates the first time a well shows a saturation change

631 Two Key Operational Model Metrics

632 After each operational model shown in Table 2 was completed, it was used to simulate the entire
633 period from zero to 200 years. The two key metrics obtained from these simulations are the
634 radius of the CO₂ plume (R_0 , where S_g and CO₂ mass fraction are at least 0.02) as a function of
635 time, and the radius at which the pressure response is big enough to drive fluid through a
636 hypothetical flow path in the caprock (R_1 , where $dP \geq 1$ bar), which occurs at the end of the
637 injection period (20 years). These two key metrics also define Area of Review (AoR) under the
638 U.S. EPA Class VI well regulation (U.S. EPA, 2013).

639 Figure 41 plots the ratio of R_0 for the operational and actual models as a function of time for each
640 operational model. A ratio less than one indicates that the operational-model plume does not
641 migrate as far updip as the actual-model plume, and this is the result for all the early operational
642 models. Later operational models under-predict plume migration at early times, but slightly over-
643 predict it at later times. Two results are shown for the initial operational model (Year 0) and the
644 twenty-five-year operational model, both of which are non-hysteretic, one with $S_{gr} = 0$ during the

post-injection period, and the other with $S_{gr} = 0.2$. The fifty-year operational model is a hysteretic model, with history-dependent S_{gr} , and as expected, its results are bracketed by the two twenty-five-year non-hysteretic models. The large difference between the ratios for the twenty-five-year non-hysteretic models (dark green curves) is one indication that using a hysteretic model helps reduce uncertainty in plume-migration prediction. If one had used the difference between the initial non-hysteretic models (pink curves) to judge the importance of including hysteresis, the small difference would have been misleading because the updip migration of the initial plume is so small (less than 20% of the actual migration) that there is little opportunity for hysteretic effects to come into play.

Figure 42 plots the ratio of R_0 for the operational and actual models for 200 years, as a function of the year the model was developed, illustrating the gradual decrease in uncertainty in CO₂ updip migration as more data are used to improve the operational model. Figure 42 also shows the analogous plot for the pressure response R_1 for 20 years, again illustrating a gradually decreasing trend in uncertainty. Generally, the trend in R_1 is similar to that for R_0 , showing that uncertainty in CO₂ plume migration and pressure response behave comparably: the initial operational model produces a poor prediction of actual model behavior, while using 1-3 years of monitoring data improves operational model predictions somewhat, and using 5 years improves them more, and by 10 years the operational model is significantly closer to the actual model. Using data collected between 10 and 25 years further improves the operational model.

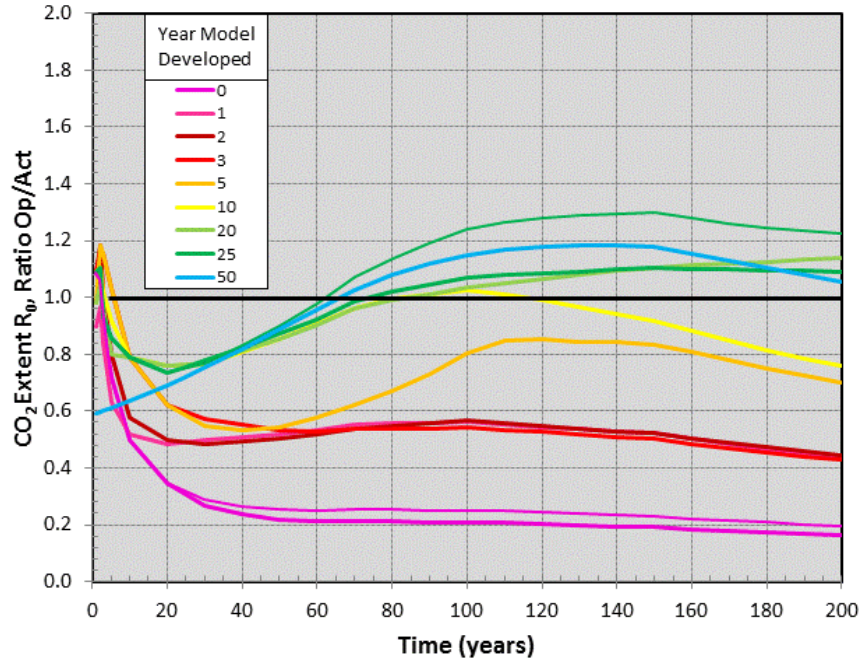


Figure 41. Ratio of the updip CO_2 plume migration R_0 for operational (Op) and actual (Act) models, as a function of time. Values less than one indicate the operational model does not move as far updip as the actual model. The legend identifies the year the operational model was developed. For the 0- and 25-year operational models, the thinner line has $S_{gr} = 0$ and the thicker line has $S_{gr} = 0.2$.

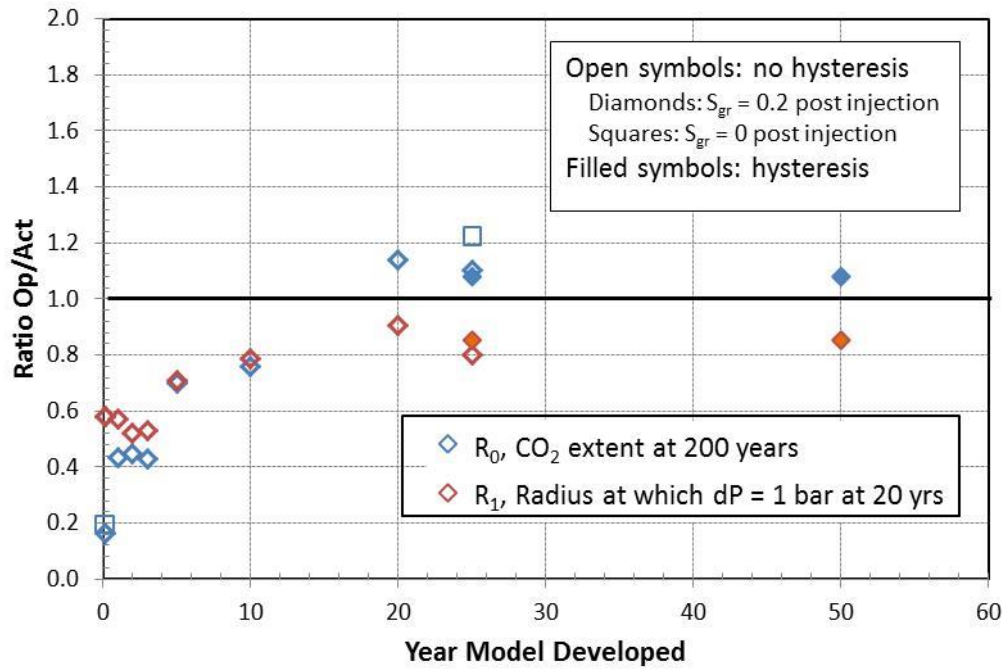


Figure 42. Ratios of R_0 and R_1 for operational (Opt) and actual (Act) models, with the horizontal axis indicating the year the operational-model was developed. Values of R_0 less than one indicate the operational-model CO_2 plume does not move as far updip as in the actual model.

674

675 **5. Discussion**

676 The hypothesis investigated in this study is that uncertainties in forecasts of CO₂ plume evolution
677 and pressure change decrease over time as more operational data are collected and incorporated
678 into operational models. The key features of the pressure transients examined (and the model
679 properties they inform) are:

- 680 • magnitude of overall pressure change (horizontal permeability)
- 681 • difference between responses at monitoring wells that are near the injection well and
682 those that are farther away (horizontal permeability)
- 683 • difference between responses at the perforated interval and at the top of the formation
684 (vertical permeability)
- 685 • curvature of the dP versus time plots (flow field geometry, storativity).

686 An important point to note about the saturation profiles is that for the operational model profiles
687 tend to show saturation peaks at the same depths, because the operational model is layered,
688 whereas the actual model shows saturation peaks at different depths, because the lateral and
689 vertical heterogeneity enables irregular fluid flow paths upward and updip through the formation
690 under buoyancy forces. Thus rather than comparing the exact depth of saturation peaks, we try to
691 match the general trend of peaks developing first at the perforated interval near the injection
692 well, and moving gradually upward and updip, which is sensitive to both horizontal and vertical
693 permeability.

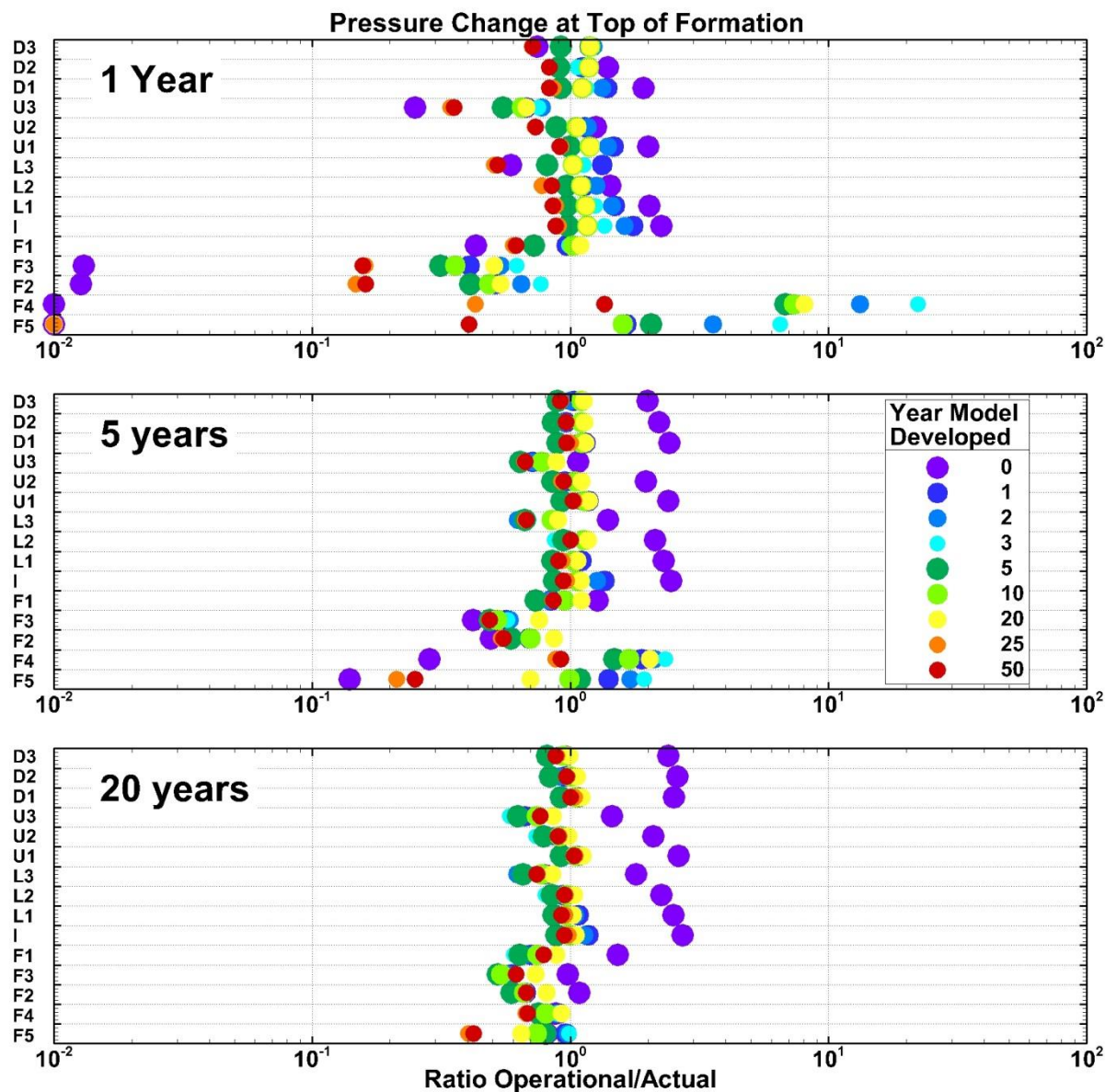
We present in Figures 43 and 44 a compact summary of the evolution of uncertainty of these key measures of GCS system changes. The plots show concordance at selected monitoring locations at three different times through the plotting of pressure change and gas saturation for the series of operational models developed over time (different colored circles) normalized by the actual values at those same locations and times. For example, the purple circle labeled with a zero would be the initial model (model developed at year zero) and the corresponding normalized results from that initial model are shown at 1 year, 5 years, and 20 years. Similarly, the dark blue, medium blue, light blue etc. circles represent the years 1, 2, 3, etc., respectively, that the model was updated. For pressure change, results at times during the CO₂ injection period are most relevant, whereas for gas saturation, results at later times (e.g., post-injection times when the CO₂ plume has reached many monitoring wells) are of more interest. Figure 43 shows that despite some scatter, there is a general trend of migration of the forecasted pressure differences in the figure toward the line where operational normalized by actual equals unity. Figure 44 shows analogous results for saturation in the top layer at three different times. The trend toward better concordance (reduced uncertainty) over time is not as clear for the saturation as for pressure because saturation is much more sensitive to local permeability heterogeneity in the model. Nevertheless, there is improvement over time at many locations, and this result mimics what would actually be observed in field data that are limited and subject to vagaries of measurement location in a heterogeneous natural system. Overall, Figures 43 and 44 make the point that uncertainty in the plume's future migration and effects on the subsurface are large at the beginning, but with competent monitoring and updating of operational models, the uncertainty trends downward over time.

Some details of the particular system we studied may be useful for cases of GCS in depleted natural gas reservoirs. For example, we observed that when both CH₄ and CO₂ are included in the model, distant monitoring wells show a distinctive signal of a CH₄ arrival presaging the CO₂ arrival. This effect has been observed and modeled previously (e.g., Oldenburg et al., 2013). We also found that the decline of saturation peaks in the post-injection period requires imbibition and capillary trapping to be properly modeled

Table 2 shows the year when the CO₂ plume reaches each monitoring well, indicating that for the first three years, CO₂ reaches only the nearest three wells (D1, L1, and U1). The CO₂ plume reaches only five wells during the first 10 years of injection, and only six wells by the end of the injection period at 20 years. This sequence suggests the idea of initially drilling only a few monitoring wells near the injection well, then adding more monitoring wells as the CO₂ plume grows. Adding one or two new monitoring wells every 5-10 years, with locations informed by previous plume development, should be a cost-effective approach to monitoring CO₂ plume migration. In contrast, the pressure-transient information provided by distant wells is useful even at early times. Thus, a good initial monitoring well configuration might consist of three nearby wells (e.g., D1, L1, U1), and one or two more distant well (e.g., F3, F4). Another possibility for minimizing the number of monitoring wells would be to augment monitoring-well observations with time-lapse geophysical surveys (e.g., Doughty and MacLennan, 2018; Pevzner et al., 2011; Daley et al., 2011).

Perfect concordance between operational and actual model pressure transients and saturation profiles is not expected given the significant lateral heterogeneity of the actual model (e.g., Figures 3 and 6) which is not included in the operational models. Of course, pressure-transient data from multiple wells can be inverted to estimate heterogeneous permeability distributions,

739 but with pressure data from only two depths (the top of the perforated interval and the top of the
740 storage formation), and local permeability values required for more than 20 model layers, this
741 would be an ill-posed inverse problem, requiring sophisticated inverse methods. Doing a joint
742 inversion of pressure-transient and saturation profile data is also a possibility, but again would
743 require advanced inverse methods. Such approaches are not in keeping with our conceptual
744 model of field operators using and updating (improving) relatively simple numerical models.
745 Instead, we acknowledge that concordance will not be perfect, and try to improve the model by
746 looking at general trends in the pressure transients and saturation profiles, as described in the
747 previous section, just as operators are expected to do.



748

749 *Figure 43. Ratio of pressure change (operational/actual) at three times for each monitoring well*
 750 *for the sequence of operational models (color identifies the year the model was developed),*
 751 *showing general evolution toward the line where operational/actual equals one. For the 0- and*
 752 *25-year non-hysteretic models, two values of residual gas saturation are shown: circles indicate*
 753 *$S_{gr} = 0$ and deltas indicate $S_{gr} = 0.2$. Symbols are slightly different sizes for better visibility of*
 754 *tightly grouped symbols.*

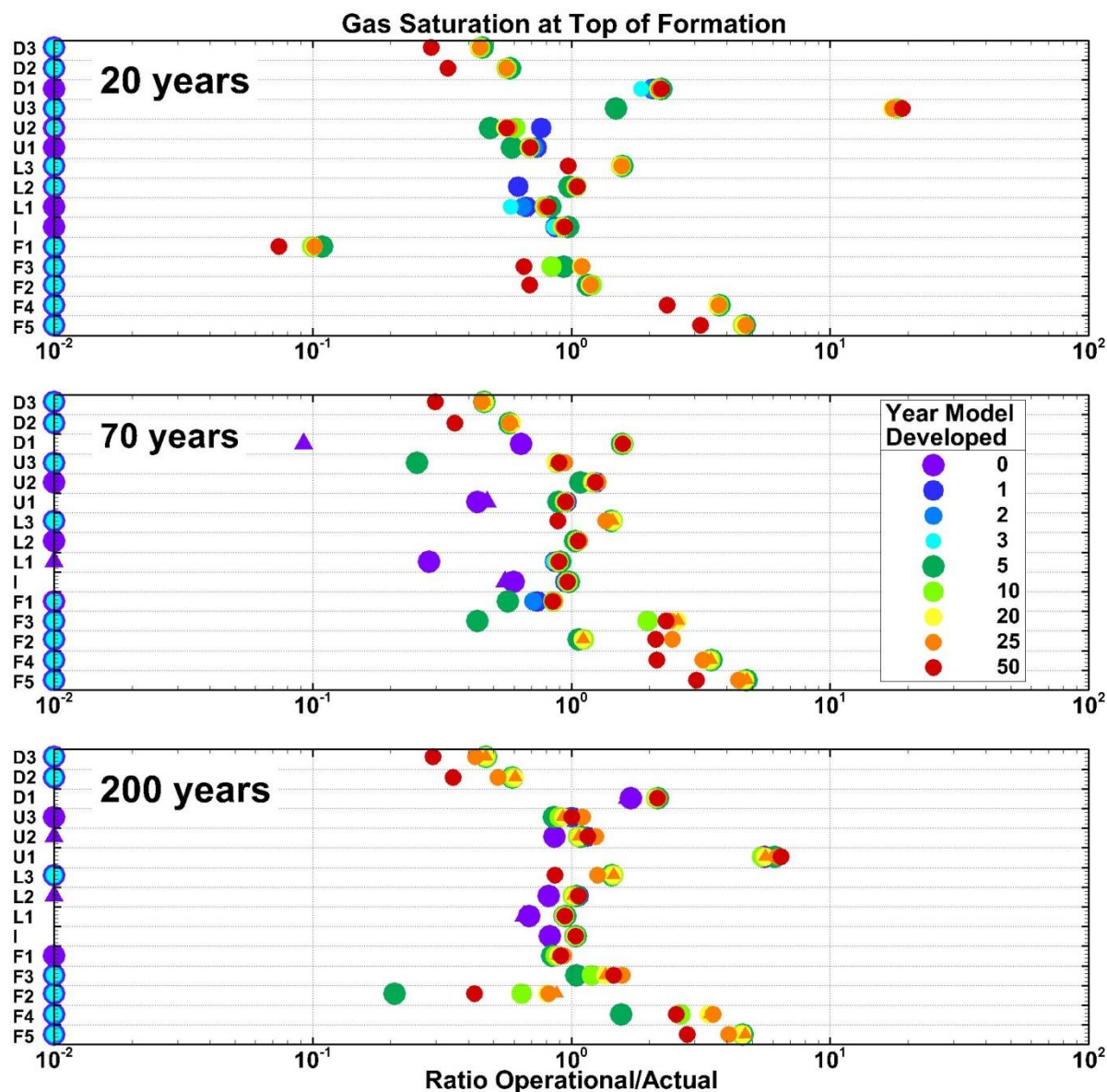


Figure 44. Ratio of saturation at top of storage formation (operational/actual) at three times for each monitoring well, for the sequence of operational models (color identifies the year the model was developed), showing general evolution toward the line where operational/actual equals one. For the non-hysteretic models, two values of residual gas saturation are shown: circles indicate $S_{gr} = 0$ and deltas indicate $S_{gr} = 0.2$. Symbols are slightly different sizes for better visibility of tightly grouped symbols.

6. Conclusions

We have illustrated the year-by-year improvement to an initially simple operational model of CO₂ sequestration in a depleted natural gas reservoir. The analysis of each year's pressure-transient and saturation-profile data provides the impetus for modifications to the operational model. Two key metrics represent the ability of the operational model to accurately predict the results of the actual model: the extent of the CO₂ plume updip migration, and the radial extent of the pressure pulse. Deviations between the actual and operational models for both of these metrics steadily decrease as more monitoring data become available over time to improve the operational model. While the goal of this paper was to show the reduction in uncertainty that occurs when models are updated and improved based on operational data, the process by which we demonstrated this reduction in uncertainty also illustrates a workflow that may a useful example for site operators.

The summary plots (Figures 41 – 44) indicate that for a twenty-year injection period, using monitoring data for the first 10 years greatly improves the ability of the operational model to predict the 50-year PISC period and out to the end of the entire 200 year simulation. In fact, data from the first year are already valuable, especially in constraining near-injection-well properties. However, including data from the post-injection period is mandatory for understanding both the drainage and imbibition aspects of CO₂ plume migration, and for the present example with a high-permeability storage formation and significant updip CO₂ migration, it was necessary to use a hysteretic model to properly account for both of these processes. Some of the parameters of the hysteretic model could be inferred from just the first five years of the post-injection period, when the saturation peaks first began to decrease, but a clearer picture emerged by considering longer post-injection times around 50 years, when saturation values neared the residual saturation.

Acknowledgements and Disclaimer

We thank Jeff Wagoner of Lawrence Livermore National Laboratory for providing the geologic model of the Southern Sacramento River Delta region, and Diana Bacon (PNNL) and Christopher Brown (PNNL) for constructive reviews of an earlier draft. This work was supported by the Assistant Secretary for Fossil Energy, Office of Sequestration, Hydrogen, and Clean Coal Fuels, for the National Risk Assessment Partnership (NRAP) project managed by the National Energy Technology Laboratory (NETL). Additional support came from the U.S. Department of Energy under Contract No. DE-AC02-05CH11231. This report was prepared as an account of work sponsored by an agency of the United States Government.

References

- Burton, E., Mateer, N., Myhre, R., and Stone, M., 2016. WESTCARB Phase III Final Report, Summary of California Activities California Energy Commission Report CEC-500-2016-053, 49 pp.
- California Air Resources Board, 2017. Carbon Capture and Sequestration Protocol under the Low Carbon Fuel Standard.
https://www.arb.ca.gov/fuels/lcfs/ccs_protocol_010919.pdf
- Chadwick, R.A. and Noy, D.J., 2015. Underground CO₂ storage: demonstrating regulatory conformance by convergence of history-matched modeled and observed CO₂ plume behavior using Sleipner time-lapse seismics. *Greenhouse Gases: Science and Technology*, 5(3), pp.305-322.
- Chen, Y. and Zhang, D., 2006. Data assimilation for transient flow in geologic formations via ensemble Kalman filter. *Advances in Water Resources*, 29(8), pp.1107-1122.
- Daley, T.M., Ajo-Franklin, J.B. and Doughty, C., 2011. Constraining the reservoir model of an injected CO₂ plume with crosswell CASSM at the Frio-II brine pilot. *International Journal of Greenhouse Gas Control*, 5(4), pp.1022-1030.
- Deutsch, C.V. and Journel, A.G., 1992. *Geostatistical Software Library and User's Guide* (2nd Ed.). Oxford University Press, New York.
- Foxall, W., Doughty, C., Lee, K.J., Nakagawa, S., Daley, T., Burton, E., Layland-Bachmann, C., Borglin, S., Freeman, K., Ajo-Franklin, J., Jordan, P., Kneafsey, T., Oldenburg, C., Ulrich, C.,

2017. Investigation of Potential Induced Seismicity Related to Geologic Carbon Dioxide Sequestration in California, California Energy Commission Report CEC-500-2017-028.

Freifeld, B.M., Trautz, R.C., Kharaka, Y.K., Phelps, T.J., Myer, L.R., Hovorka, S.D. and Collins, D.J., 2005. The U-tube: A novel system for acquiring borehole fluid samples from a deep geologic CO₂ sequestration experiment. *Journal of Geophysical Research: Solid Earth*, 110(B10).

Harp, D.R., Oldenburg, C.M. and Pawar, R., 2019. A metric for evaluating conformance robustness during geologic CO₂ sequestration operations. *International Journal of Greenhouse Gas Control*, 85, pp.100-108.

Keating, E.H., Doherty, J., Vrugt, J.A. and Kang, Q., 2010. Optimization and uncertainty assessment of strongly nonlinear groundwater models with high parameter dimensionality. *Water Resources Research*, 46(10), W10517.

Le Guénan, T., Gravaud, I., De Dios, C., Gavilanes, L., Poletto, F., Eguilior, S. and Hurtado, A., 2018, October. Determining performance indicators for linking monitoring results and risk assessment—application to the CO₂ storage pilot of Hontomín, Spain. In *The Greenhouse Gas Control Technologies-GHGT-14*.

Doughty, C. and MacLennan, K., 2018. Using TOGA to model CO₂-EOR in conjunction with time-lapse electromagnetic monitoring, TOUGH Symposium 2018, Lawrence Berkeley National Lab., Berkeley CA, October 8-10.

Oladyshkin, S., Class, H., Helmig, R. and Nowak, W., 2011. A concept for data-driven uncertainty quantification and its application to carbon dioxide storage in geological formations. *Advances in Water Resources*, 34(11), pp.1508-1518.

Oldenburg, C.M., 2018. Are we all in concordance with the meaning of the word conformance, and is our definition in conformity with standard definitions? *Greenhouse Gases: Science and Technology*, 8(2), pp.210-214.

Oldenburg, C.M., Doughty, C. and Spycher, N., 2013. The role of CO₂ in CH₄ exsolution from deep brine: Implications for geologic carbon sequestration. *Greenhouse Gases: Science and Technology*, 3(5), pp.359-377.

Oldenburg, C.M., Pruess, K. and Benson, S.M., 2001. Process modeling of CO₂ injection into natural gas reservoirs for carbon sequestration and enhanced gas recovery. *Energy & Fuels*, 15(2), pp.293-298.

Pevzner, R., Shulakova, V., Kepic, A. and Urosevic, M., 2011. Repeatability analysis of land time-lapse seismic data: CO₂CRC Otway pilot project case study. *Geophysical Prospecting*, 59(1), pp.66-77.

866 Sun, A.Y., Morris, A.P. and Mohanty, S., 2009. Sequential updating of multimodal
867 hydrogeologic parameter fields using localization and clustering techniques. *Water Resources*
868 *Research*, 45(7), W07424.

869

870 U.S. EPA (United States Environmental Protection Agency), 2008. Federal Requirements under
871 the Underground Injection Control (UIC) Program for Carbon Dioxide (CO₂) Geologic
872 Sequestration (GS) Wells, Proposed Rule, 40 CFR Parts 144 and 146, EPA-HQ-OW-2008-0390.
873

874 U.S. EPA, Geologic Sequestration of Carbon Dioxide Underground Injection Control (UIC)
875 Program Class VI Well Area of Review Evaluation and Corrective Action Guidance Office of
876 Water (4606M), EPA 816-R-13-005, May 2013.

877

878 van Genuchten, M.Th., 1980. A closed-form equation for predicting the hydraulic conductivity
879 of unsaturated soils. *Soil Science Society of America Journal*, 44(5), pp. 892-898.

880

881 Walter, L., Binning, P.J., Oladyshkin, S., Flemisch, B. and Class, H., 2012. Brine migration
882 resulting from CO₂ injection into saline aquifers—An approach to risk estimation including
various levels of uncertainty. *International Journal of Greenhouse Gas Control*, 9, pp.495-506.